RBM7 deficiency promotes breast cancer metastasis by coordinating MFGE8 splicing switch and NF-kB pathway

Fang Huang[1†], Zhenwei Dai[1†], Jinmiao Yu[1†], Kainan Wang[†2], Chaoqun Chen[1], Dan Chen[3], Jinrui Zhang[4], Jinyao Zhao[4], Wenjing Zhang[4], Yangfan Qi[4*], Yang Wang[1*]

[1]Sino-US Research Center for Cancer Translational Medicine of the Second Affiliated Hospital of Dalian Medical University & Institute of Cancer Stem Cell, Dalian Medical University, Dalian 116023, China

[2]Department of Oncology & Sino-US Research Center for Cancer Translational Medicine, the Second Affiliated Hospital, Dalian Medical University, Dalian 116023, China

[3]Department of Pathology, the First Affiliated Hospital of Dalian Medical University, Dalian Medical University, Dalian 116011, China

[4]Institute of Cancer Stem Cell, Dalian Medical University, Dalian 116044, China

[†] These authors contributed equally to this work.

[*] Correspondence:

Yang Wang; Sino-US Research Center for Cancer Translational Medicine of the Second Affiliated Hospital of Dalian Medical University & Institute of Cancer Stem Cell, Dalian Medical University, Dalian 116023, China; Tel: +86-411-86110531; Email:

21 yangwang@dmu.edu.cn

22 Yangfan Qi; Institute of Cancer Stem Cell, Dalian Medical University, Dalian, China

23 116044; Tel: +86-411-86110531; Email: yangfanqi@dmu.edu.cn

24

25

26 Running title: RBM7 presents anti-metastasis activity by regulating splicing

27

28

29 We declare no conflict of interest on the studies described in this manuscript.

Abstract

Aberrant alternative splicing is well-known to be closely associated with tumorigenesis of various cancers. However, the intricate mechanisms underlying breast cancer metastasis driven by deregulated splicing events remain largely unexplored. Here, we unveiled RBM7 as a novel regulator of alternative splicing that plays a crucial role in counteracting the metastatic potential of breast cancer. Through bioinformatics analysis and IHC staining validation, we revealed that RBM7 is decreased in lymph node and distant organ metastases of breast cancer as compared to primary lesions. Furthermore, we found that low expression of RBM7 is correlated with the reduced disease-free survival of breast cancer patients. Breast cancer cells with RBM7 depletion exhibited an increased potential for lung metastasis compared to scramble control cells. The absence of RBM7 stimulated breast cancer cell migration, invasion, and angiogenesis. Mechanistically, RBM7 regulates the splicing of MFGE8 directly, favoring the production of the predominant MFGE8-L isoform. This results in the attenuation of STAT1 phosphorylation and alterations in cell adhesion molecules. The MFGE8-L isoform exerted an inhibitory effect on the migratory and invasive capability of breast cancer cells, while the MFGE8-S isoform had the opposite effect. Particularly, the ectopic expression of MFGE8-L significantly reversed the pro-invasion effect of RBM7 silencing, but did not contribute to the promotion of angiogenesis-related secreted proteins. In RBM7 depleted cells, a gene set enrichment analysis revealed a significant amplification of the NF-κB cascade. Concordantly, RBM7 negatively regulates p65 phosphorylation. Furthermore, an NF-κB inhibitor could obstruct the increase in

HUVEC tube formation caused by RBM7 silencing. Clinically, we noticed a positive correlation between RBM7 expression, MFGE-8 exon7 inclusion, and p65 downstream targets. Therefore, our study not only offer mechanistic insights into how abnormal splicing contributes to the aggressiveness of breast cancer, but also provide a new approach for molecular-targeted therapy in combating breast cancer.

Keywords: RBM7; alternative splicing; breast cancer; metastasis

Introduction

Alternative splicing (AS) emerges as a substantial contributor to the production of a myriad of transcripts from limited genes, which enriched protein variation and phenotypic diversity in multicellular organisms. Pre-mRNA splicing reactions require a step-wise assembly of spliceosome, a megadalton complex that recognize consensus regulatory sequences, including 5' and 3' splice sites marking exon-intron boundary, and the branch point site (BPS), to accomplish exon definition (Shi, 2017) (Wilkinson, Charenton et al., 2020). While a splice site is suboptimal, AS emerges under control of inherent sequence acting in cis, namely exonic or intronic splicing enhancer or silence, and the cognate trans-acting splicing factors, which can strengthen or weaken the recognition of splice sites by spliceosome.

It is well documented that AS dysregulation leads to multiple human diseases, including cancer (Montes, Sanford et al., 2019) (Singh & Cooper, 2012). Tumorigenicity has been linked with cancer-specific splicing switch arising from either cis-elements mutations or deregulated splicing regulatory factors. In some cases, splicing factors, particularly spliceosomal components SF3B1 and U2AF1, are frequently mutated across diverse cancer types (Baralle, 2005) (Harbour, Roberson et al., 2013) (Smith, Choudhary et al., 2019) (Cheruiyot, Li et al., 2021). For instance, recurrent SF3B1 mutations led to retention of intronic region in BRD9 pre-mRNA, conferring loss of core subunit function to the ncBAF chromatin remodeling complex and metastatic advantage to melanoma cells (Inoue, Chew et al., 2019). Another layer of regulation involves the abnormal expression of splicing factors derived from altered

83 regulatory pathway. As an archetypal example, a set of members in SR protein family
84 such as SRSF1 and SRSF3 are upregulated in breast tumors, lung tumors, glioma and
85 exhibit oncogenic ability via altering AS products (for example, Bcl-x, MYO1B,
86 NUMB and p53) (Anczuków, Akerman et al., 2015) (Zhou, Wang et al., 2019) (Tang,
87 Horikawa et al., 2012) (Zhou, Gong et al., 2020). Otherwise, many splicing factors such
88 as RBM proteins can either functions as oncoproteins or tumor suppressors in cancer-
89 type dependent manner (Li, Guo et al., 2021), which may be attributed to tissue-specific
90 AS patterns.

91 Breast cancer is the most common diagnosed malignancy and remain the second
92 leading cause of cancer mortality (over 41,000 deaths annually in the USA) among
93 females worldwide (Siegel, Miller et al., 2019). Metastasis to vital organs accounts for
94 approximately 90% cancer-related death. The 5-year overall survival rate of patients
95 with metastatic breast cancer is drastically decreased to about 25%, as compared to the
96 primary cancer patients' prognosis with a survival rate greater than 80% (Rabbani &
97 Mazar, 2007) (Valastyan & Weinberg, 2011). Despite advances in early diagnosis and
98 comprehensive interventions for breast cancer treatment, limited effective strategy
99 against metastasis has been an outstanding challenge for improving prognostication of
100 patients. This highlights the urgent need for deepened understanding of mechanisms
101 underlying development of metastasis. Tumor metastasis is multi-step process
102 involving a sequential cascade of events, such as epithelial-mesenchymal transition
103 (EMT), local invasion from primary tumor site, lymphogenic or hematogenic
104 dissemination, cancer cells seeding and metastatic lesions formation (Liang, Zhang et

105 al., 2020). AS dysregulation has been implicated in multistage process of metastasis.
106 For example, the switch of CD44 or FGFR2 splicing isoforms can lead to EMT
107 phenotype (Chen, Zhao et al., 2018) (Warzecha, Sato et al., 2009). VEGF-A or XBP1
108 splicing transition is tightly linked to angiogenesis in cancer (Bates, 2008) (Zeng, Xiao
109 et al., 2013). On account of the phenotypic plasticity in metastatic cells conferred by
110 alternative splicing, further investigation in potential role of critical splicing regulatory
111 factors and the associated splicing events in breast cancer metastasis is warranted.

112 RNA-binding proteins (RBPs) are a large class of conserved proteins that
113 participate in cancer development through precisely control RNA metabolism,
114 including RNA splicing. RBM7, a member of RBP family, is commonly known to exert
115 RNA surveillance activity as a component of the human nuclear exosome target (NEXT)
116 complex (Meola, Domanski et al., 2016) . Aberrant expression of RBM7 is not only
117 associated with lung fibrosis onset and motor neuronopathy, but also impacts cancer
118 cell proliferation (Fukushima, Satoh et al., 2020) (Xi, Zhang et al., 2020). Previous
119 findings have established a direct connection of RBM7 with spliceosome factors SF3B2
120 and SF3B4 (Falk, Finogenova et al., 2016), yet whether RBM7 is involved in the
121 regulation of AS remain elusive. In this study, we report that RBM7 is frequently
122 reduced in a subset of breast cancer metastases from lymph nodes lesions and distant
123 organ as compared to primary tumors and its low expression predicts dismal survival
124 outcomes of patients. Breast cancer cells with loss of RBM7 gain enhanced aggressive
125 capability and metastatic potential. Mechanistically, RBM7 ablation enhanced the
126 splicing switch of MFG-E8 pre-mRNA from canonical isoform MFGE8-L to a

127 truncated isoform MFGE8-S. Ectopic expression of MFGE8-L caused marked
128 suppression of migratory and invasive ability of breast cancer cells, whereas MFGE8-
129 S showed opposite function/ disabled such function. At another layer, RBM7
130 discordantly regulated the phosphorylation of p65. In concert, NF-κB inhibitor
131 abolished pro-angiogenesis effect of RBM7 ablation in breast cancer. Above all, our
132 findings uncovered a previously unidentified role of RBM7 in breast cancer metastasis
133 via coupling MFGE8 splicing switch and NF-κB signaling activation, suggesting a new
134 therapeutic target and prognostic predictor for breast cancer.
135
136

137 **Results**

138 **RBM7 is reduced in metastatic lesions of breast cancer and positively correlated**

139 **with patients' prognosis**

140 To determine the clinical relevance of RBM7 in breast cancer, we assessed the
141 correlation between RBM7 and important clinical outcomes. Analysis of TCGA, GEO
142 and the METABRIC breast cancer datasets showed that RBM7 expression positively
143 correlates with overall survival of breast cancer patients (Figure 1A and Supplementary
144 Figure 1A-1B). RBM7 low expression predicts the reduced disease-free survival in
145 patients with breast cancer (Figure 1B and Supplementary Figure 1C). Congruently, we
146 found RBM7 is decreased in breast cancer compared to normal tissues (Figure 1C and
147 Supplementary Figure 1D). Further dissection in a cohort of breast cancer patients from
148 the cBioPortal unveiled cases with lymph node metastasis have lower expression of
149 RBM7 as compared to cases without metastasis (Figure 1D). We next performed
150 immunohistochemistry (IHC) detection of RBM7 in breast cancer tissue microarrays.
151 The results showed that patients bearing clinical stage III tumors have significantly
152 decreased RBM7 expression than patients bearing I and II clinical stage tumors (Figure
153 1E). In tissue chip containing triple negative breast cancer, the more aggressive and
154 mesenchymal breast cancer subtype, RBM7 exhibits reduced protein levels in tumors
155 as compared to paracancer tissues (Figure 1F). In addition, we collect specimen
156 consisted of tumor tissues from 21 breast primary cancer, in 9 cases, from metastatic
157 loci and took advantage of IHC analysis to determine the RBM7 expression. Most (25%
158 strong positive;67% moderate positive) of primary tumor samples displayed a positive

159 IHC staining for RBM7, whereas most of lung/liver metastatic lesions showed weak or
160 negative RBM7 expression (Figure 1G). We also obtained paired primary breast cancer
161 and lymph node metastatic loci and found, when compared to the corresponding
162 primary tumor, the expression of RBM7 is significantly decreased in lymph node
163 metastases (Figure 1H-1I). These results associated RBM7 with breast cancer
164 metastasis, prompting us to further investigate the functional role of RBM7 in
165 metastatic processes of breast cancer.
166

167 **RBM7 silencing provokes metastatic potential of breast cancer**

168 In light with the above findings, we generated RBM7-silenced breast cancer cells
169 using lentiviral expression of short hairpin RNA (shRNA) followed by profiling high-
170 throughput transcriptome by RNA sequencing. Strikingly, Gene Ontology and pathway
171 analysis displayed a wide range of RBM7-regulated genes were enriched in
172 extracellular matrix organization, cell migration and angiogenesis (Figure 2A-2B),
173 which have been characterized as crucial processes in tumor metastasis. A heatmap
174 generated from qRT-PCR analysis of differentially expressed genes in RBM7-depleted
175 breast cancer cells verified that a series of metastasis-related genes were upregulated
176 upon RBM7 knockdown (Figure 2C). The lung metastasis is one of the most prevalent
177 distant metastases that breast cancer is prone to and associated with poor prognosis of
178 patients (Medeiros & Allan, 2019). Thus, we performed tail-vein transfer model to
179 evaluate the potential impact of RBM7 on pulmonary metastasis of breast cancer cells.
180 5×10^4 4T1 cells, the mouse breast cancer cell line simulating stage IV human breast

181 tumor, with stable RBM7 silence or control vector were implanted into BALB/c mice
182 via tail vein. After 3 weeks, RBM7-silenced 4T1 cells were able to develop more
183 spontaneous lung metastases than control cells as judged by pulmonary nodules number
184 and haematoxylin-eosin (HE) staining of lung tissues (Figure 2D-2F and
185 Supplementary 2A). Cancer metastasis is comprised of a complex cascade of events,
186 such as migration, invasion and angiogenesis, thus we next to determine which process
187 is mediated by RBM7-loss in facilitating breast cancer metastasis. We utilized transwell
188 chamber with or without matrix coat and would healing assays to examine the potential
189 function of RBM7 in migration and invasion capabilities and found the depletion of
190 RBM7 led to a visible increase in mobility and invasiveness of both the triple-negative
191 breast cancer (TNBC) cell line MDA-MB-231, estrogen receptor positive breast cancer
192 cell line MCF7 and 4T1 cells (Figure 2G-2H and Supplementary 2B-2E). Conversely,
193 RBM7 overexpression notably repressed MDA-MB-231 and MCF7 cells to migrate or
194 invade across transwell inserts (Figure 2I-2J). Similar results were obtained in two
195 additional TNBC cell lines BT549 and HCC1937 (Supplementary 2F-2G), which
196 proved that RBM7 possessed the capability to suppress the migration and invasion of
197 breast cancer cells. To examine the impact of RBM7 on angiogenesis in breast cancer,
198 we cultured human umbilical vein endothelia cells (HUVEC) with condition medium
199 obtained from culture supernatants of RBM7-depleted or scramble shRNA transduced
200 cells for tube formation analysis. Compared to the scramble control, HUVEC incubated
201 with culture medium from RBM7-knockdown breast cancer cells exhibited accelerated
202 tube formation length and branch junction (Figure 2K), suggesting the inhibitory effect

203 of RBM7 on breast cancer angiogenesis. Taken together, the above data demonstrated
204 RBM7 as tumor suppressor by regulating breast cancer migration, invasion and
205 angiogenesis.
206
207 **RBM7 exhibits splicing regulatory function in breast cancer**
208 In previous studies, RBM7 is commonly characterized as an RNA-binding
209 constituent of trimeric NEXT complex, which directs the RNA exosome to non-coding
210 transcriptome for degradation (Lubas, Andersen et al., 2015). However, the
211 mechanistical role of RBM7 in cancer remain largely unknown. Intriguingly, we
212 observed that, attributed to the ablation of RBM7, almost 551 splicing events occurred
213 significant decrease in PSI (percent splicing inclusion), whereas 289 splicing events
214 endured increased PSI (Figure 3A). The changed events were divided among various
215 types of AS (alternative splicing), including SE (skipping exon), IR (intron retention),
216 A5SS (alternative 5' splice site), A3SS (alternative 3' splice site), and MXE (mutually
217 exclusive exons), of note, SE events were the most prominently regulated (Figure 3B).
218 A majority of AS events in particular of SE and A5SS category were in decrease of PSI
219 upon RBM7 depletion (Figure 3C-3D), indicating that the presence of RBM7 may
220 promote the usage of alternative splice sites. Subsequently, we extracted the candidate
221 binding motifs which reside within cassette exons or A5SS and found UUUCUU motfs,
222 simiar to RBM7 binding site (polyU) were enriched in RBM7 positively regulated AS
223 events to a greater extent that control exons unimpacted by RBM7 (Figure 3E), raising
224 the possibility that RBM7 may serve as a splicing activator through directly tethering

225 cis-element in pre-mRNA. This is coherent with the nuclear localization of RBM7 in
226 breast cancer cells (Supplementary 3A). In order to explore the splicing regulation
227 activity of RBM7 in distinct pre-mRNA context, we validated a series of RBM7-
228 significantly-changed splicing events across different AS types according to the RNA-
229 seq results. The RT-PCR analysis demonstrated that the PSI of selected gene related to
230 cancer progression was either increased or decreased endogenously upon RBM7
231 depletion (Figure 3F and Supplementary 3B). Considering that the AS is a sophisticated
232 multi-step reaction that is regulated by both pre-mRNA-interacting splicing factor and
233 other assistant factors in a context-dependent manner (Wright, Smith et al., 2022), we
234 doubted the divergent effect of RBM7 on distinct splicing targets was due to a more
235 complicated mechanism. Gene ontology (GO) enrichment analysis identified a majority
236 of genes undergoing AS alterations were involved in cytoskeleton assembly and
237 organization (Figure 3G). While globally analyzing the network enrichment of RBM7-
238 regulated downstream splicing events, we observed its targets are functionally
239 connected to well-linked network containing gene subgroups (Figure 3H), which are
240 associated with biological processes in tumor cell metastasis, again suggesting the
241 cancer-related function of RBM7.
242

243 **RBM7 depletion switches splicing outcomes of MFG-E8 by decreasing MFG-E8-**
244 **L isoform**

245 To ascertain the functional targets that explain the inhibitory role of RBM7 in
246 breast cancer metastasis, we examined RNA immunoprecipitation -seq for RBM7 and

247 RNA-seq data for breast cancer cells expressing two shRNAs targeting RBM7. Venn
248 diagram illustrating overlapping genes pointed forward a hotspot gene, namely MFGE8
249 (Figure 4A). We focused on the AS control of MFGE8 by RBM7 resulting in a
250 significant alteration in ratio of MFGE8 two isoforms, of which the canonical isoform
251 (MFGE8-L) has been demonstrated to be correlated with tumor formation and
252 aggressiveness of breast cancer (Yang, Hayashida et al., 2011). Importantly, the exon 7
253 located in F5/8 type C 2 domain, which is obligated to bind to phosphatidylserine, was
254 lacked in the short isoform of MFGE8 (Figure 4B). Further RT-PCR identification
255 verified RBM7 ablation indeed potentiated the production of MFGE8 short splice
256 variant (MFGE8-S) in various TNBC cell lines (Figure 4C). Similar results were
257 obtained from MCF7 cells, suggesting that RBM7 regulated the AS of MFGE8
258 independently of the ER status. In separate experiments, we transfected breast cancer
259 cells with an exogenous MFGE8 splicing reporter containing exon 6-8 and 600bp of
260 flanking intron sequences to determine the splicing regulatory function of RBM7.
261 Accordingly, the depletion of RBM7 still induced the splicing shift of the minigene
262 reporter by elevating MFGE8-S variant (Figure 4D). To test whether such splicing
263 regulatory effect was directly or indirectly, we analyzed the sequence of alternative
264 exon 7 and the motifs nearby its 5' or 3' splice sites, and found two poly(U) motifs are
265 positioned in proximal to the pseudo 3' splice site. Subsequent RT-PCR assay for the
266 precipitation in RIP assays confirmed RBM7 could bind to the upstream sequence
267 containing UUUCUU motifs adjacent to 3' splice site of MFGE8 cassette exon, but not
268 another region nearby it (Figure 4E). To pinpoint the location for the potential cis-

269 element for AS regulation by RBM7, we designed antisense oligonucleotides (ASOs),
270 which have been chemically modified to avoid endogenous nuclease degradation
271 without recruiting RNase H, to block the UUUCUU residues in proximity to
272 intron6/exon7 junction. As shown in Figure 4F, when compared to control ASO,
273 treatment with ASOs targeting the potential binding site (UUUCUU) of RBM7,
274 contributed to the exclusion of exon7, further suggesting that RBM7 regulated the
275 exon7 skipping of MFGE8 by directly binding to its pre-mRNA.
276

277 **The short variant of MFGE8 abolishes the inhibitory function of its classical**
278 **isoform on breast cancer cell migration and invasion**

279 MFGE8 encodes a secreted protein, Milk fat globule-EGF factor 8 (MFG-E8),
280 which participates in a variety of cellular processes, including mammary gland
281 branching morphogenesis, angiogenesis and mucosal healing, etc (Raymond, Ensslin
282 et al., 2009). We applied MFGE8-L stably overexpressing- or depleted-breast cancer
283 cells to transwell assays and observed the cellular migratory and invasive capabilities
284 was visibly suppressed by MFGE8-L overexpression (Supplementary 4A-4B). On the
285 contrary, the knockdown of MFGE8-L provoked cell migration and invasion
286 (Supplementary 4C). Strikingly, while MDA-MB-231 or HCC1937 expressing
287 MFGE8-L showed a remarkable decrease in migratory and invasive ability compared
288 to control vector, MFG-E8-S not only totally abolished the inhibitory function of
289 MFGE8-L but elicited modest pro-migration/ invasion actions on breast cancer cells
290 (Figure 5A and Supplementary 4D-4E). In comparison with MFG-E8 containing N-

291 terminal EGF-like domain and C-terminal twice-repeated F5/8 type C domains, the
292 protein encoded by MFGE8-S loses the second F5/8 type C domain, implying a
293 shortage of the function corresponding to membrane-binding. Immunofluorescence
294 assays revealed the MFGE8-L forms foci in cytoplasm, particularly enriched near cell-
295 cell contact sites, whereas MFGE8-S is more evenly distributed in the nucleus and
296 cytoplasm (Figure 5B). Furthermore, we compared transcriptome profiles between
297 MFGE8-L and MFGE8-S ectopically expressing breast cells and found a set of
298 functional genes were down-regulated by MFGE8-L, whereas this negative regulation
299 was abrogated in response to MFGE8-S (Figure 5C). The differentially expressed genes
300 between two splice variants were predominantly enriched in cell adhesion molecules
301 and JAK-STAT cascade as revealed by KEGG pathway and Gene ontology analysis
302 (Figure 5D). Subsequent experimental validation demonstrated that the activation of
303 STAT1 was hindered by MFGE8-L, but not affected by MFGE8-S (Figure 4E).
304 Considering that STAT1 signaling activation plays an important role in tumor cell
305 metastasis via cell adhesion molecules induction (Marimuthu, Lakshmanan et al., 2022)
306 (Chen, Hao et al., 2019), it is highly plausible that MFGE8-L, but not MFGE8-S,
307 impeded breast cancer cell motility and invasive capability in a STAT1-dependent
308 manner.
309
310 **RBM7 depletion-stimulated aggressiveness of breast cancer is dependent on**
311 **MFGE8 splicing switch and NF-kB pathway activation**
312 Next, we sought to assess if MFGE8 splicing switch is responsible for acquisition

313 of aggressive feature in RBM7-silenced breast cancer cells. Flag-tagged MFG-E8-L or
314 an empty vector was co-expressed in MDA-MB-231 cells together with RBM7 shRNA
315 (Supplementary Figure 5A). Following seeding into transwell chamber, cells
316 transfected with RBM7 shRNA exerted a higher migratory and invasive capability than
317 scramble control, consistent with above data. Importantly, the restoration of MFGE8-L
318 expression diminished the acquired aggressive properties of MDA-MB-231 cells
319 resulted from RBM7 depletion (Figure 6A). Similar results were obtained using RBM4-
320 depleted MCF7 cells with or without MFGE8-L complement (Figure 6B). However, a
321 series of shRBM7-upregulated secreted factors that have been reported to drive tumor
322 angiogenesis (Gopinathan, Milagre et al., 2015) (Fousek, Horn et al., 2021) (Feng, Ke
323 et al., 2019), were not impacted by MFGE8-L/S (Supplementary Figure 5B and Figure
324 6C). Condition medium derived from breast cancer cells overexpressing MFGE8-L/S
325 showed negligible effect on HUVEC tube formation (Supplementary Figure 5C),
326 implying that there exists additional mechanism underlying breast cancer metastasis
327 attributed to RBM7 reduction.

328 Given that consecutive gene set enrichment analysis (GESA) of highest-ranking
329 gene sets based on transcriptomic profile of mRNA expression showed a signature for
330 NF-κB pathway that was augmented upon depletion of RBM7 (Figure 6D), we
331 suspected that the transcriptional activation of downstream genes in NF-κB signaling
332 known to facilitate tumor angiogenesis might be involved in shRBM7-exerted pro-
333 metastatic function. As expected, the phosphorylation of p65, a core transcription factor
334 well-known to switch on NF-κB pathway was notably enhanced by RBM7 knockdown,

335 meanwhile, IκBα phosphorylation that can blockade p65 activation was curbed upon
336 RBM7 knockdown (Figure 6E). Conversely, RBM7 overexpression impeded the
337 activation of p65 (Supplementary Figure 5D). Yet MFGE8-L/S had no effect on
338 phosphorylation of p65 or IκBα (Supplementary Figure 5E). We further carried out
339 Matrigel tube formation assays and found NF-κB inhibitor PDTC drastically reversed
340 the promotion of HUVEC angiogenesis by conditional medium harvested from RBM7-
341 depleted cells (Figure 6F-6G), implying that RBM7-p65 axis may participate in
342 HUVEC angiogenesis through reprogramming the secretome of breast cancer cells.
343 Similar effect was observed with respect to cell motility and invasion (Supplementary
344 Figure 5F). Taken together, these data above indicated that both MFGE8 splice switch
345 and NF-κB pathway activation are required for mediating the pro-metastasis activity of
346 RBM7 reduction in breast cancer.
347

348 **The PSI of MFGE-8 exon 7 is decreased in breast cancer patients and positively**
349 **correlated with RBM7 expression**

350 To study the clinical relevance of MFGE-8 isoform switch, we analyzed the PSI
351 changes of cassette exon7 in TCGA breast cancer cohort and found exon7 skipping
352 occurs more frequently in tumor than in normal tissues (Figure 7A). Consistently, in
353 comparison with normal counterparts, the splicing of MFGE8 is shifted towards a
354 reduced proportion of MFGE8-L across multiple cancer types, including LUAD, HNSC,
355 COAD, etc (Supplementary 6A). RT-PCR assay was performed in surgical tumor
356 specimens in breast cancer patients and showed MFGE8 exon7 is prone to skipping in

357 tumor (Figure 7B). On the other hand, the splicing switch in lymph node metastases
358 favored MFGE exon7 exclusion when compared to paired primary tumor tissues from
359 3 breast cancer patients (Figure 7C). This is coherent with decreased RBM7 expression
360 levels found in breast cancer with lymph node metastasis. In addition, patients with
361 high expression of MFGE8 exon7 had a visibly better overall survival than patients
362 with low expression (Figure 7D). We performed Pearson correlation test and revealed
363 a noticeably positive correlation between the expression of RBM7 and exon7 inclusion
364 of MFGE8 in breast cancer (Figure 7E), further supporting MFGE8 isoform switch
365 regulated by RBM7.
366
367

368 **Discussion**

369 Previous reports have recognized the RNA-binding protein RBM7 as a component
370 of the NEXT complex that could facilitate RNA exosome targeting to a subset of non-
371 coding RNAs and aberrant transcripts (Meola et al., 2016) (Pascal Preker, 2008),
372 including short-lived exosome substrates and pre-mRNAs, for surveillance and
373 turnover . In addition to this specific characteristic, RBM7 was shown to interact with
374 subunits of 7SK snRNP complex and thus activate P-TEF downstream genes in
375 response to DNA damage (Bugai, Quaresma et al., 2019). Herein, we discover a novel
376 role of RBM7 in alternative splicing control through directly binding to its cognate cis-
377 element in pre-mRNA. Using whole-transcriptome sequencing, we found the depletion
378 of RBM7 contributed to exon exclusion in approximately 70% SE/A5SS events,
379 implying RBM7 mainly functions as a splicing activator in breast cancer. However, the
380 increase of PSI also occurred due to RBM7 knockdown in a smaller faction of splicing
381 events, such as ZMYND8. We speculated this converse impact may be associated with
382 the intrinsically sophisticated splicing processes driven by distinct core splicing factors,
383 cognate cis-acting element and co-factors in a context-dependent manner (e.g., pre-
384 mRNA structure, base modification, antagonistic or cooperative effect of multiple
385 splicing factors). Similar to many splicing factors, like SR proteins and hnRNPs, RBM7
386 has an RRM-domain required for target RNA recognition in the N-terminus. Through
387 ectopic expression of a series of RBM7 truncated mutant, we unveiled the disordered
388 region (162-266) rich in polar residues serves as the functional modular to execute
389 alternative splicing program.

390 Currently, the pathobiological function of RBM7 in breast cancer is underexplored
391 except one study that claimed an oncogenic role of RBM7 since its knockdown
392 inhibited breast cancer cell proliferation (Xi et al., 2020). Nevertheless, in our study,
393 RBM7 knockdown in breast cancer displayed visibly pro-metastasis function with
394 activated NF-κB signaling. More importantly, according to TCGA database (total cases >
395 1000 used for analysis), RBM7 shows decreased expression in breast cancer,
396 particularly in the metastasis loci and has positive correlation with patients' survival
397 outcomes. It is therefore highly doubtful that RBM7 could serve as an oncogene in
398 breast cancer as previously reported. Moreover, we can't exclude additional biological
399 function of RBM7 in breast cancer. RBM7-targeted silencing for breast cancer would
400 likely be detrimental for neighbouring heathy tissue and immune environment as a
401 result of NF-κB-dependent pro-inflammatory mediators and cytokines secretion.
402 Other splicing events switch triggered by RBM7 might also be linked to tumor
403 development. For example, we found RBM7 regulated alternative splicing of AKT2,
404 which is involved in glucose metabolism (Hay, 2011). Further investigation is
405 warranted to elaborate more splicing mechanisms of RBM7 in breast cancer.

406 In conclusion, we discovered that down-regulated RBM7 and its cognate elevated
407 exon7-exclusion MFGE8 were tightly related to enhanced breast cancer metastatic
408 potential and poor prognosis of patients. MFGE8-L, the canonical variant, possessed
409 the capability to trigger STAT1 phosphorylation and inhibit the motility and invasion
410 of breast cancer cells, whereas splice switch to MFGE8-S was found loss-of-function
411 for this tumor-suppressive role. At another layer, RBM7 reduction led to NF-κB

412 pathway activation, resulting in enhancement of breast tumor aggressiveness. Overall,
413 our findngs implicated that activated NF-κB pathway worked in concert with MFGE8
414 splicing transition to spur metastasis in RBM7-depleted breast cancer. Additionally,
415 although the detailed clinical significance underlying their cooperation need further in-
416 depth investigation, we propose that RBM7 and its regulated splicing variants might
417 serve as potential therapeutic biomarker and prognostic indicator in breast cancer
418 patients.
419
420

Reference

Anczuków O, Akerman M, Cléry A, Wu J, Shen C, Shirole Nitin H, Raimer A, Sun S, Jensen Mads A, Hua Y, Allain Frédéric HT, Krainer Adrian R (2015) SRSF1-Regulated Alternative Splicing in Breast Cancer. *Molecular Cell* 60: 105-117

Baralle D (2005) Splicing in action: assessing disease causing sequence changes. *Journal of Medical Genetics* 42: 737-748

Bates SJHaDO (2008) VEGF-A splicing: the key to anti-angiogenic therapeutics? *NATURE REVIEWS* 7

Bugai A, Quaresma AJC, Friedel CC, Lenasi T, Düster R, Sibley CR, Fujinaga K, Kukanja P, Hennig T, Blasius M, Geyer M, Ule J, Dölken L, Barborič M (2019) P-TEFb Activation by RBM7 Shapes a Pro-survival Transcriptional Response to Genotoxic Stress. *Molecular Cell* 74: 254-267.e10

Chen C, Zhao S, Karnad A, Freeman JW (2018) The biology and role of CD44 in cancer progression: therapeutic implications. *Journal of Hematology & Oncology* 11

Chen Y, Hao X, Sun R, Wei H, Tian Z (2019) Natural Killer Cell–Derived Interferon-Gamma Promotes Hepatocellular Carcinoma Through the Epithelial Cell Adhesion Molecule–Epithelial-to-Mesenchymal Transition Axis in Hepatitis B Virus Transgenic Mice. *Hepatology* 69: 1735-1750

Cheruiyot A, Li S, Nonavinkere Srivatsan S, Ahmed T, Chen Y, Lemacon DS, Li Y, Yang Z, Wadugu BA, Warner WA, Pruett-Miller SM, Obeng EA, Link DC, He D, Xiao F, Wang X, Bailis JM, Walter MJ, You Z (2021) Nonsense-Mediated RNA Decay Is a Unique Vulnerability of Cancer Cells Harboring SF3B1 or U2AF1 Mutations. *Cancer Research* 81: 4499-4513

Falk S, Finogenova K, Melko M, Benda C, Lykke-Andersen S, Jensen TH, Conti E (2016) Structure of the RBM7–ZCCHC8 core of the NEXT complex reveals connections to splicing factors. *Nature Communications* 7

443 Feng P-C, Ke X-F, Kuang H-L, Pan L-L, Ye Q, Wu J-B (2019) RETRACTED ARTICLE: BMP2
444 secretion from hepatocellular carcinoma cell HepG2 enhances angiogenesis and tumor growth in
445 endothelial cells via activation of the MAPK/p38 signaling pathway. *Stem Cell Research & Therapy* 10
446 Fousek K, Horn LA, Palena C (2021) Interleukin-8: A chemokine at the intersection of cancer plasticity,
447 angiogenesis, and immune suppression. *Pharmacology & Therapeutics* 219
448 Fukushima K, Satoh T, Sugihara F, Sato Y, Okamoto T, Mitsui Y, Yoshio S, Li S, Nojima S, Motooka D,
449 Nakamura S, Kida H, Standley DM, Morii E, Kanto T, Yanagita M, Matsuura Y, Nagasawa T,
450 Kumanogoh A, Akira S (2020) Dysregulated Expression of the Nuclear Exosome Targeting Complex
451 Component Rbm7 in Nonhematopoietic Cells Licenses the Development of Fibrosis. *Immunity* 52: 542-
452 556.e13
453 Gopinathan G, Milagre C, Pearce OMT, Reynolds LE, Hodivala-Dilke K, Leinster DA, Zhong H,
454 Hollingsworth RE, Thompson R, Whiteford JR, Balkwill F (2015) Interleukin-6 Stimulates Defective
455 Angiogenesis. *Cancer Research* 75: 3098-3107
456 Harbour JW, Roberson EDO, Anbunathan H, Onken MD, Worley LA, Bowcock AM (2013) Recurrent
457 mutations at codon 625 of the splicing factor SF3B1 in uveal melanoma. *Nature Genetics* 45: 133-135
458 Hay N (2011) Akt isoforms and glucose homeostasis – the leptin connection. *Trends in Endocrinology*
459 *& Metabolism* 22: 66-73
460 Inoue D, Chew G-L, Liu B, Michel BC, Pangallo J, D'Avino AR, Hitchman T, North K, Lee SC-W,
461 Bitner L, Block A, Moore AR, Yoshimi A, Escobar-Hoyos L, Cho H, Penson A, Lu SX, Taylor J, Chen
462 Y, Kadoch C et al. (2019) Spliceosomal disruption of the non-canonical BAF complex in cancer. *Nature*
463 574: 432-436
464 Li Z, Guo Q, Zhang J, Fu Z, Wang Y, Wang T, Tang J (2021) The RNA-Binding Motif Protein Family in

Cancer: Friend or Foe? *Frontiers in Oncology* 11

Liang Y, Zhang H, Song X, Yang Q (2020) Metastatic heterogeneity of breast cancer: Molecular mechanism and potential therapeutic targets. *Seminars in Cancer Biology* 60: 14-27

Lubas M, Andersen Peter R, Schein A, Dziembowski A, Kudla G, Jensen Torben H (2015) The Human Nuclear Exosome Targeting Complex Is Loaded onto Newly Synthesized RNA to Direct Early Ribonucleolysis. *Cell Reports* 10: 178-192

Marimuthu S, Lakshmanan I, Muniyan S, Gautam SK, Nimmakayala RK, Rauth S, Atri P, Shah A, Bhyravbhatla N, Mallya K, Grandgenett PM, Hollingsworth MA, Datta K, Jain M, Ponnusamy MP, Batra SK (2022) MUC16 Promotes Liver Metastasis of Pancreatic Ductal Adenocarcinoma by Upregulating NRP2-Associated Cell Adhesion. *Molecular Cancer Research* 20: 1208-1221

Medeiros B, Allan AL (2019) Molecular Mechanisms of Breast Cancer Metastasis to the Lung: Clinical and Experimental Perspectives. *International Journal of Molecular Sciences* 20

Meola N, Domanski M, Karadoulama E, Chen Y, Gentil C, Pultz D, Vitting-Seerup K, Lykke-Andersen S, Andersen Jens S, Sandelin A, Jensen Torben H (2016) Identification of a Nuclear Exosome Decay Pathway for Processed Transcripts. *Molecular Cell* 64: 520-533

Montes M, Sanford BL, Comiskey DF, Chandler DS (2019) RNA Splicing and Disease: Animal Models to Therapies. *Trends in Genetics* 35: 68-87

Pascal Preker JN, Susanne Kammler, Søren Lykke-Andersen, Marianne S. Christensen, Christophe K. Mapendano, Mikkel H. Schierup, Torben Heick Jensen (2008) RNA Exosome Depletion Reveals Transcription Upstream of Active Human Promoters. *SCIENCE* 322: 4

Rabbani SA, Mazar AP (2007) Evaluating distant metastases in breast cancer: from biology to outcomes. *Cancer and Metastasis Reviews* 26: 663-674

487 Raymond A, Ensslin MA, Shur BD (2009) SED1/MFG-E8: A Bi-Motif protein that orchestrates diverse
488 cellular interactions. *Journal of Cellular Biochemistry* 106: 957-966
489 Shi Y (2017) Mechanistic insights into precursor messenger RNA splicing by the spliceosome. *Nature*
490 *Reviews Molecular Cell Biology* 18: 655-670
491 Siegel RL, Miller KD, Jemal A (2019) Cancer statistics, 2019. *CA: A Cancer Journal for Clinicians* 69:
492 7-34
493 Singh RK, Cooper TA (2012) Pre-mRNA splicing in disease and therapeutics. *Trends in Molecular*
494 *Medicine* 18: 472-482
495 Smith MA, Choudhary GS, Pellagatti A, Choi K, Bolanos LC, Bhagat TD, Gordon-Mitchell S, Von
496 Ahrens D, Pradhan K, Steeples V, Kim S, Steidl U, Walter M, Fraser IDC, Kulkarni A, Salomonis N,
497 Komurov K, Boultwood J, Verma A, Starczynowski DT (2019) U2AF1 mutations induce oncogenic
498 IRAK4 isoforms and activate innate immune pathways in myeloid malignancies. *Nature Cell Biology* 21:
499 640-650
500 Tang Y, Horikawa I, Ajiro M, Robles AI, Fujita K, Mondal AM, Stauffer JK, Zheng ZM, Harris CC
501 (2012) Downregulation of splicing factor SRSF3 induces p53β, an alternatively spliced isoform of p53
502 that promotes cellular senescence. *Oncogene* 32: 2792-2798
503 Valastyan S, Weinberg Robert A (2011) Tumor Metastasis: Molecular Insights and Evolving Paradigms.
504 *Cell* 147: 275-292
505 Warzecha CC, Sato TK, Nabet B, Hogenesch JB, Carstens RP (2009) ESRP1 and ESRP2 Are Epithelial
506 Cell-Type-Specific Regulators of FGFR2 Splicing. *Molecular Cell* 33: 591-601
507 Wilkinson ME, Charenton C, Nagai K (2020) RNA Splicing by the Spliceosome. *Annual Review of*
508 *Biochemistry* 89: 359-388

Wright CJ, Smith CWJ, Jiggins CD (2022) Alternative splicing as a source of phenotypic diversity. *Nature Reviews Genetics* 23: 697-710

Xi P-W, Zhang X, Zhu L, Dai X-Y, Cheng L, Hu Y, Shi L, Wei J-F, Ding Q (2020) Oncogenic action of the exosome cofactor RBM7 by stabilization of CDK1 mRNA in breast cancer. *npj Breast Cancer* 6

Yang C, Hayashida T, Forster N, Li C, Shen D, Maheswaran S, Chen L, Anderson KS, Ellisen LW, Sgroi D, Schmidt EV (2011) The Integrin αvβ3-5 Ligand MFG-E8 Is a p63/p73 Target Gene in Triple-Negative Breast Cancers but Exhibits Suppressive Functions in ER+ and erbB2+ Breast Cancers. *Cancer Research* 71: 937-945

Zeng L, Xiao Q, Chen M, Margariti A, Martin D, Ivetic A, Xu H, Mason J, Wang W, Cockerill G, Mori K, Li JY-s, Chien S, Hu Y, Xu Q (2013) Vascular Endothelial Cell Growth–Activated XBP1 Splicing in Endothelial Cells Is Crucial for Angiogenesis. *Circulation* 127: 1712-1722

Zhou X, Wang R, Li X, Yu L, Hua D, Sun C, Shi C, Luo W, Rao C, Jiang Z, Feng Y, Wang Q, Yu S (2019) Splicing factor SRSF1 promotes gliomagenesis via oncogenic splice-switching of MYO1B. *Journal of Clinical Investigation* 129: 676-693

Zhou Z, Gong Q, Lin Z, Wang Y, Li M, Wang L, Ding H, Li P (2020) Emerging Roles of SRSF3 as a Therapeutic Target for Cancer. *Frontiers in Oncology* 10

529 **Materials and Methods**

530 **Cell culture**

531 Human breast cancer cell lines (MDA-MB-231, MCF7, HCC1937 and BT-549) and
532 human embryonic kidney cell HEK293T in this article were obtained from the
533 American Type Culture Collection (ATCC). MDA-MB-231 cells were cultured without
534 carbon dioxide at 37°C in Leibovitz's L-15 medium (Gibco) contained 10% FBS
535 (SINSAGE TECH). MCF7 and HEK293T cells were cultured with DMEM mediun
536 (Gibco) supplemented with 10% FBS. HCC1937 cells were cultured with RPMI-1640
537 media (Gibco) supplemented with 10% FBS, while BT-549 was maintained with RPMI-
538 1640 media (Gibco) supplemented with 10% FBS and 0.023 U/ml insulin. HUVECs
539 were cultured with Endothelial Cell Medium (ScienCell) supplemented with ECGS
540 (ScienCell), P/S solution (ScienCell) and 10% FBS (ScienCell). Except for MDA-MB-
541 231, all the cells above were cultured in a 37 °C humidified incubator.

542 **Constructions of stable cell lines**

543 To generate RBM7 overexpression vector, the coding regions of this gene
544 (NM_016090.4) were cloned into pCDH-CMV-MCS-EF1-Puro with N-terminal Flag
545 tag. For RBM7 knockdown, target-specific shRNA (RBM7-sh1: 5'-
546 CGAAAGGACTATGGATAACAT-3';RBM7-sh2:5'-
547 CTACCTAGCAGATAGACATTA-3') was cloned into pLKO.1 vector. And HEK293T
548 cells were transfected these over-expression (or low-expression) lentivirus plasmis
549 together with lentivirus packaging plasmids pPAX2 and pMD2 according to the
550 manufacturer's instructions. Viruses were collected 48 hours after transfection and then

551 to infect breast cancer cell line with 8 ug/ml polybrene (beyotime biotechnology) for
552 24 hours. Positive cells were selected with 3 ug/ml puromycin.

553 **Western Blot assay**

554 Cells were lysed with RIPA buffer (10 mM Tris-HCl pH 7.5, 150 mM NaCl, 0.1% SDS,
555 1% Triton X-100, and 1% sodium deoxycholate) supplemented with protein tyrosine
556 phosphatase inhibitor Na_3VO_4 (1mM), serine protease inhibitor PMSF (1mM) and
557 protease inhibitor Cocktail. Immunoblotting assay was performed using standard
558 methods. The following antibodies were used: anti-RBM7 (Sigma-Aldrich,
559 HPA013993), anti-Flag (Sigma-Aldrich, F1804), anti-GAPDH (Proteintech, 10494-1-
560 AP), anti-Phospho-Akt (Ser473) (Cell Signaling Technology, #4060), anti-Akt (pan)
561 (Cell Signaling Technology, #4691), anti-Phospho-NF-κB p65 (Cell Signaling
562 Technology, #3033), anti-NF-κB p65(Cell Signaling Technology, #8242), anti-IκBα
563 (Cell Signaling Technology, #4814), anti-Phospho-IκBα (Ser32) (Cell Signaling
564 Technology, #2859), anti-Phospho-stat1 (Tyr701) (Cell Signaling Technology,
565 #8062),and anti-MFGE8(R&D systems, MAB2767). Used secondary antibodies were
566 conjugated to horseradish peroxidas. The protein bands were detected with an ECL
567 Enhanced chemiluminescence regent Kit (NCM, Biotech), visualized using the
568 MiniChemi™ Cheminescent image system (Beijing Sage Creation, China).

569 **RNA isolation, RNA sequencing, and PCR**

570 Total RNA from cells and tumor tissues was extracted using Trizol (Invitrogen)
571 according to the manufacturer's instructions. Total mRNA was cleaned up using
572 RNeasy Lipid Tissue Mini Kit (Qiagen, USA). And RNA-seq was carried out on

573 platform of Novogene Illumina sequencing. cDNAs were obtained using *Evo M-MLV*
574 Plus 1st Strand cDNA Synthesis Kit (Accurate Biotechnology, AG11615) with random
575 primers. qRT-PCR was carried out using MonAmp™ Universal ChemoHS Specificity
576 Plus qPCR Mix. GAPDH mRNA was examined as control for normalization. Gene
577 expression relative to GAPDH was calculated using the formula $2^{-\Delta\Delta CT}$. For identified
578 alternative splicing events, primers of the upstream and downstream of variable exons
579 or introns were designed and PCR assay was performed. PCR products were subject to
580 DNA agarose gel electrophoresis. AS events change of percent-spliced-in (PSI) values
581 were the ratio of retained splices to total transcripts. The amount of each splicing
582 isoform was measured with ImageJ. All the primers are showed in Table1.

583 **Migration and invasion assays**

584 For transwell migration assay, 10×10^4 MDA-MB-231 or other breast cancer cells
585 (MCF7, BT-549 and HCC1937) were plated in the upper chamber of 6.5 mm insert
586 (Costar, USA) with 8.0 μm polycarbonate membrane with 100 μL serum-free medium.
587 For invasion assay, 10×10^4 breast cancer cells were seeded in the top chamber of each
588 Matrigel-coated insert (BD Biosciences, USA). After 24 hours or 48 hours of
589 incubation at 37 °C, migrated or invaded cells were fixed with 4% PFA and stained in
590 0.1% crystal violet. The cell number was counted by ImageJ software in 3 views from
591 3 independent experiments.

592 **Wound healing**

593 Knockdown RBM7 in MDA-MB-231 and 4T1 cells or control cells were implanted
594 into 6-well culture dishes. When the cells grew about 90% confluence, lines of the same

595 width were drawn on the bottom of the culture dish using autoclaved sterile tips. Images
596 were captured at 0 and 36 hours after the wounding. Data shown were representative of
597 three independent repeats.

598 **Tube formation of HUVECs assay**

599 Capillary tube formation assay was used to observe angiogenesis of HUVECs.
600 HUVECs were seeded into 48-well plate coated with growth factor reduced Matrigel
601 (BD Biosciences). HUVECs cells were treated with conditioned medium for 4-5 hours
602 and then formation of capillary-like tubes was observed and stained with calcein for 30
603 minutes. Images of blood vessels were taken using fluorescence microscopy. And the
604 tube length was analyzed by ImageJ software.

605 **Immunofluorescence assay**

606 After seeded on coverslips for 36 hours, the MDA-MB-231 cells were immersion fixed
607 with 4% PFA for 20 minutes at room temperature, washed 3 times in PBS. Then the
608 cells were treated with 0.2 % Triton-X100 in PBS for 10 minutes and blocked with 3%
609 BSA for 10 minutes. Next the cells were immersed in primary antibody at 4°C overnight,
610 washed in PBS 3 times for 5 minutes each, and incubated with secondary antibody
611 labelled with Alexa fluorophore 488/592 for 1 hour at RT. After washing 3 times in
612 PBS, the cells were dyed with DAPI. In addition, antibodies targeting RBM7 (Sigma,
613 HPA013993), and Flag (Sigma, 3165) were used in the assay. The pictures are captured
614 with fluorescent microscope (Leica, USA).

615 **RNA immunoprecipitation assay**

616 RNA immunoprecipitation was performed as previously described. In brief, HEK293T

617 cells were transfected Flag-RBM7 or control plasmid. After 48 hours of transfection,
618 Flag-RBM7 or control cells were collected and cross-linked by 1% formaldehyde,
619 homogenized in lysis buffer (50 mM Tris-HCl Ph 7.5, 0.4 M NaCl, 1 mM EDTA, 1mM
620 DTT, 0.5% TritonX-100, 10% Glycerol supplemented with RNase inhibitor and broad-
621 spectrum protease inhibitors Cocktail), and broke with an ultrasonic crusher. And
622 solubilized cell lysate was obtained and precleared by ProteinG-agarose beads together
623 with nonspecific tRNA to remove nonspecific binding. Then binding RNAs with RBM7
624 protein were precipitated with Anti-Flag M2 Affinity beads. Co-precipitated RNAs
625 were subject to RT-PCR. Input controls (total RNAs) and Flag-controls were assayed
626 simultaneously to prove that the detected signals were the result of RNAs specifically
627 binding to RBM7. The gene-specific primers were designed MFGE8-RIP1-F:5'-
628 tatttatgccccctcaccgc-3'; MFGE8-RIP1-R:5'-atggtggctgcctgtaat-3';MFGE8-RIP2-F:5'-
629 ctgaggctcacccaagtag-3';MFGE8-RIP2-R:5'-GTAGGATGCCACAAACTG-3').
630 GAPDH mRNA was as negative control (GAPDH-F 5'-GGGGAAGGTGAAGGTCG-
631 G-3'; GAPDH-R 5'-TTGAGGTCAATGAAGGGG-3').

632 **Antisense oligonucleotide (ASO)-mediated splicing blockade**

633 MFGE8-ASOs were synthesized with a full-length phosphorothioate backbone and 2'-
634 O-methyl modified ribose molecules (GenScriptBiotech Corp). ASO was transfected at
635 final concentration of 100 nM using Lipofectamine3000 (Thermo Fisher Scientific)
636 according to the manufacturer's instructions. The MCF7 cells were harvested for RNA
637 and splicing assays 48 h after transfection.

638 **Animal experiments**

639 All procedures and experimental protocols involving mice were approved by the
640 Institutional Animal Care and Use Committee (IACUC) of Dalian Medical University.
641 Male NYG mice (6 weeks old, 4-5 mice per group as indicated in figures and/or figure
642 legends) were injected into tail vein with murine 4T1 breast cancer cells (6×10^5 cells)
643 to develop mice model of pulmonary metastasis. After about 2 weeks, all mice were
644 euthanized, and lungs were harvested, fixed and paraffin embedded. After lungs were
645 H&E stained, the number of metastatic lesions were enumerated by pathologist using
646 brightfield microscopy.

647 **Clinical tissues samples collection**

648 All human breast cancer tissues or normal tissue were obtained with written informed
649 consent from patients or their guardians prior to participation in the study. The
650 Institutional Review Board of the Dalian Medical University approved use of the tumor
651 specimens in this study.

652 **Statistical analyses**

653 Statistical analyses and statistical graphs were conducted by GraphPad Prism 8
654 software. To compare the differences between the two variables, Student's T-test, one-
655 way ANOVA with Dunnett multiple comparisons, and one-way ANOVA with Tukey's
656 multiple comparisons according to the specific situation were applied. $*p < 0.05$,
657 $**p < 0.01$, $***p < 0.001$, and $****p < 0.0001$ indicated the significant difference.

658

659 **Data availability**

660 The authors declare that all the data supporting the findings of this study are available

within the article and its supplementary information files. RNA-seq data in this study have been deposited in Gene Expression Omnibus of NCBI with the accession code GSE248938.

Author contributions

YW and YQ conceived the project and designed the experiments. FH, JY, ZD, KW, and DC performed most of the experiments, whereas CC, JZhang, JZhao and WZ performed data analysis. YW and YQ wrote the manuscript.

Acknowledgements

This work was supported by the National Key R&D Program of China (2022YFA1104002 to YW); the National Natural Science Foundation of China (82225034, 81830088 to YW; 82103148 to YQ; 81872247 to WZ); the Science and Technology Innovation Foundation of Dalian (2022JJ11CG009 to YW), Liaoning Revitalization Talents Program XLYC1802067 to YW; the Department of Science and Technology of Liaoning Province (2021JH6/10500160 to YW); the Basic Scientific Research Project of Education Department of Liaoning Province (LJKQZ2021104 to YQ); the Science and Technology Innovation Talent Support Program of Dalian (2022RQ056 YQ); Dalian High Level Talents Renovation Supporting Program (2019RQ097 to WZ).

Study Approval

The Institutional Animal Care and Use Committee of the Dalian Medical University approved use of animal models in this study. All human tumor tissues were obtained

683 with written informed consent from patients or their guardians prior to participation in
684 the study. The Institutional Review Board of the Dalian Medical University approved
685 use of the tumor specimens in this study
686
687

688 **Figures and figure legends**

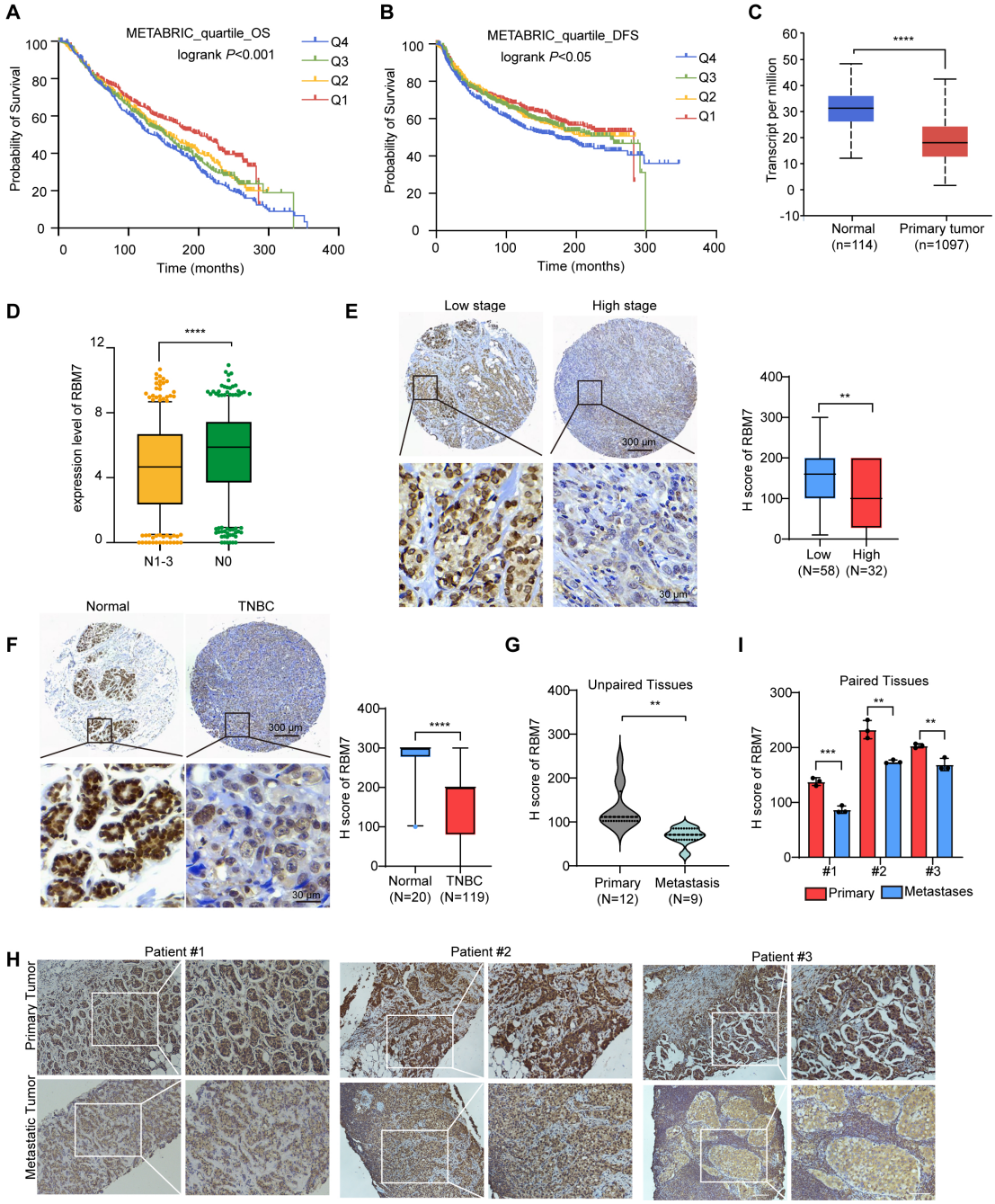

689

690 **Figure 1. Decreased RBM7 expression was associated with poor prognosis of**

691 **breast cancer.** (A-B) The correlation between RBM7 mRNA expression and overall

692 survival (OS) and disease-free-survival (DFS) of breast cancer patients (n=1980) based

693 on the METABRIC dataset. The samples were divided into four equal parts, containing

694 lower quartile Q1, median quartile Q2, upper quartile Q3 and higher quartile Q4

695 according to the expression of RBM7. (C) RBM7 mRNA level was analyzed in primary
696 breast carcinoma (n=1097) and normal tissues (n=114) from the UALCAN dataset. (D)
697 RBM7 expression level was analyzed in breast invasive carcinoma based on nodal
698 metastasis status from TCGA dataset. BRCA samples were classified into N0 (No
699 regional lymph node metastasis) (n=515), and metastases in axillary lymph node (N1-
700 N3) (n=565). (E) Representative images of IHC staining with RBM7 expression in high
701 (n=32) and low (n=58) clinical stages in breast cancer tissue microarray. Scale bars =
702 300 μm (top) or 30 μm (bottom). (F) Representative images of IHC staining with RBM7
703 expression in Triple-Negative Breast Cancer (n=119) and para-carcinoma tissue (n=20)
704 in our tissue microarray. Scale bars = 300 μm (top) and 30 μm (bottom). (G)
705 Quantitative analysis of RBM7 expression by IHC staining in primary breast cancer
706 (n=12) and unpaired metastatic cancer (n=9). (H-I) Representative immunostaining
707 images of RBM7 in 3 paired primary breast cancer and lymphatic metastasis. Scale bars
708 = 100 μm. The p value was obtained by log-rank test (A, B), and unpaired Student's T
709 test (C, D, E, F, G, I). Data are presented as means ± SD.
710

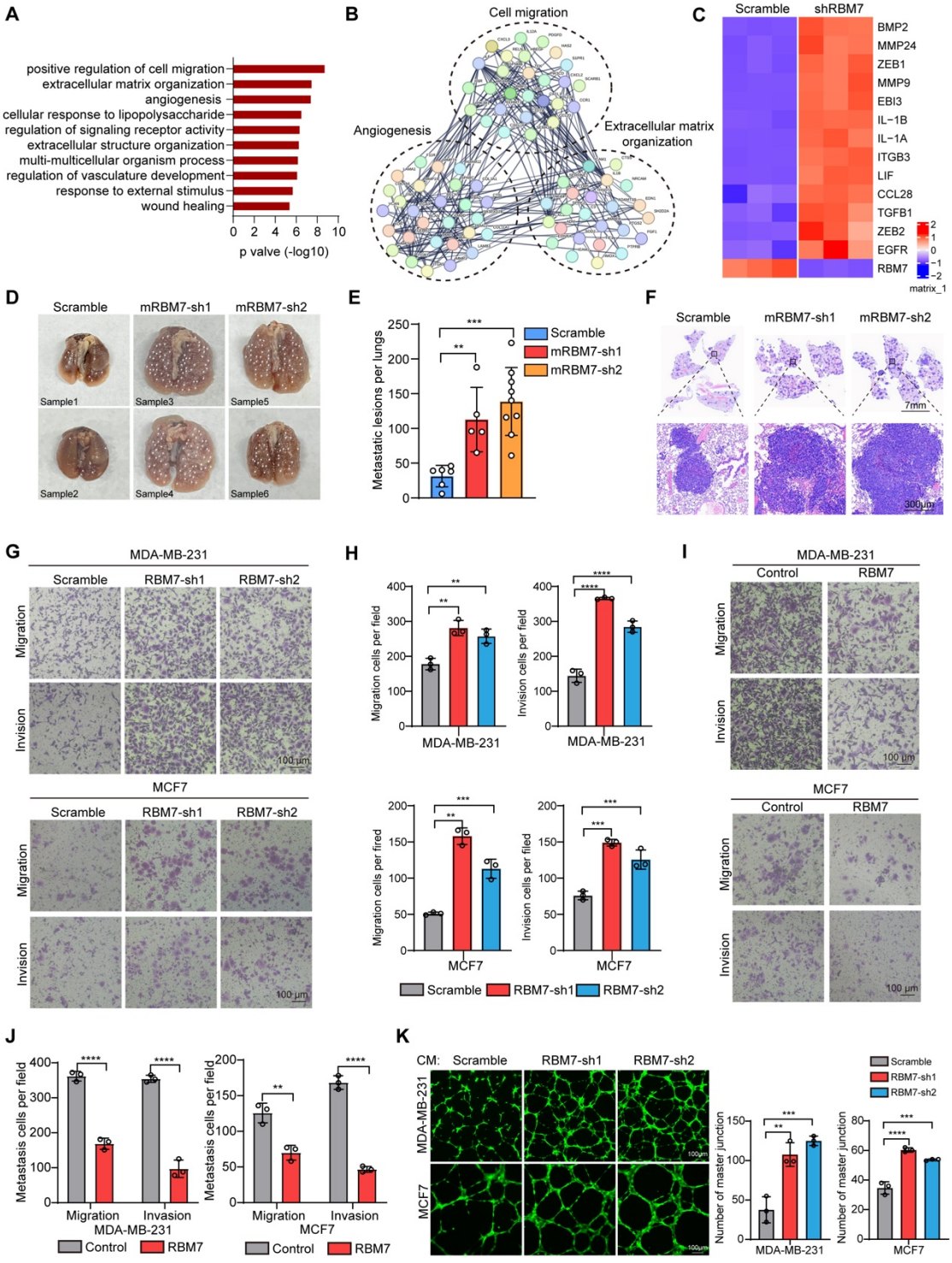

711

712 **Figure 2. RBM7 negatively regulated breast cancer metastatic potential.** (A) Gene

713 Ontology analysis showed the significantly affected biological process upon RBM7

714 knockdown in MDA-MB-231 cells. (B) Functional association network of RBM7-

715 regulated targets. The genes were analyzed using the STRING database, and subgroups

are marked according to their function. (C-E) 4T1 cells without or with RBM7 knockdown were injected into tail vein of immunodeficient NYG mice to establish a lung metastasis model. And spontaneous pulmonary metastases were assessed after about 2 weeks. (C)The white arrow indicates lung lesions macroscopically. (D) H&E stained lung sections were quantified for the number of spontaneous metastatic lesions from NYG mice (n=6, 5 and 9). Data are mean ± SD. P values were determined by one-way ANOVA with Dunnett's multiple comparisons test. (E) Representative images of H&E stained lung sections are shown. Scale bars=7 mm (top) and 300 μm (bottom). (F-I) The metastatic ability of RBM7 for breast cancer cells was evaluated by Transwell assay. Data are mean ± SD from three random fields. P values were determined by unpaired Student's T test (I) or one-way ANOVA with Dunnett's multiple comparisons test (G). (J) Representative images of the tube formation of HUVEC cells, treated with conditional medium, which cultured RBM7-KD cells and control cells for 48h and collected. Scale bars: 100 μm. Quantification of master junction was by imageJ software.

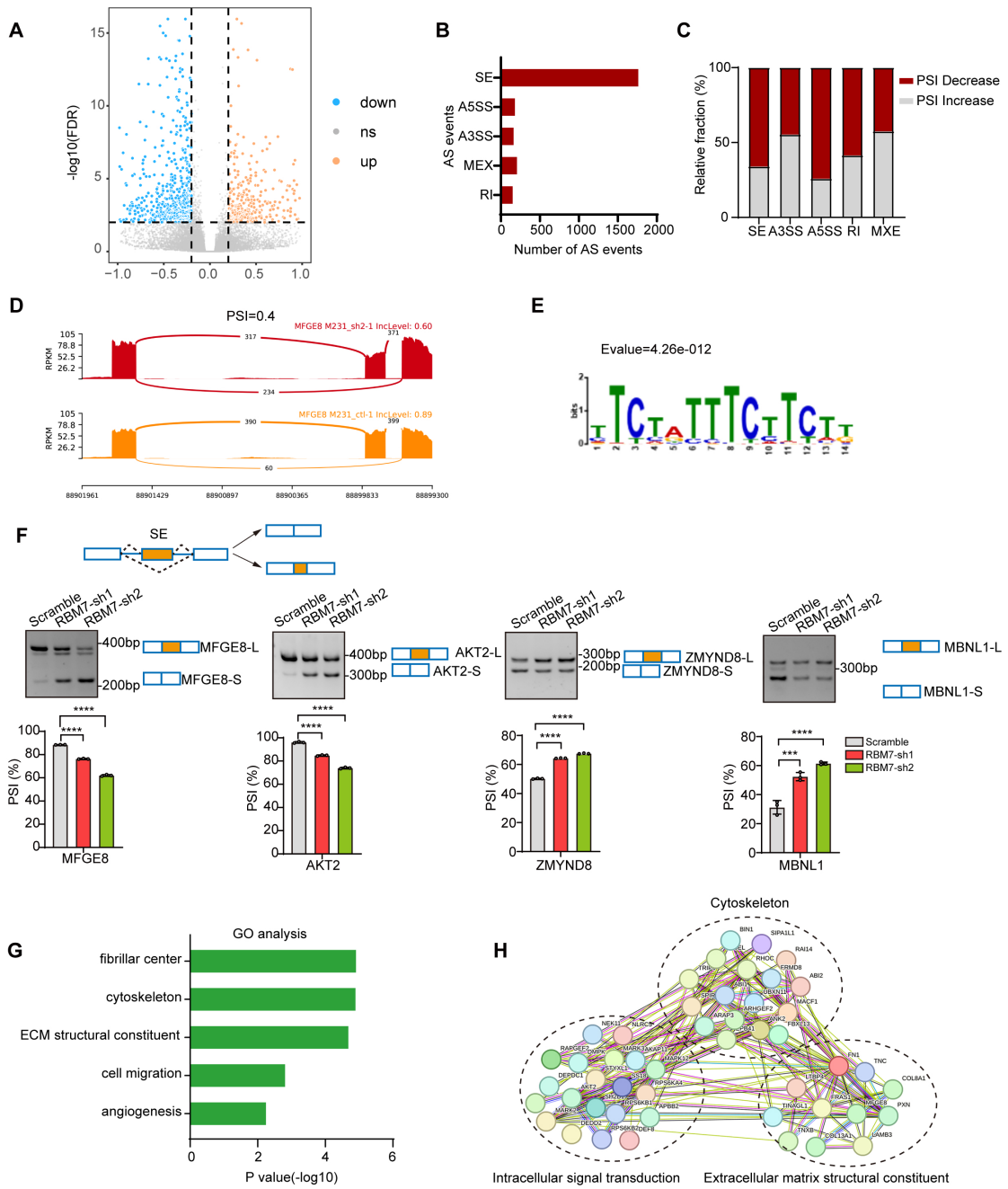

Figure 3. Global identification of alternative splicing events regulated by RBM7. (A-E) RNA-seq was performed on RBM7-knockdown MDA-MB-231 cells or control cells. And changes in splicing events were analyzed. (A) Volcano plot illustrating alternative splicing events regulated by RBM7. (B) Quantification of the different AS events affected by RBM7. (C) The relative fraction of each AS event affected positively or negatively by RBM7. (D) Examples of alternative exons affected by RBM7.

752 Alternative splicing of MFGE8 was chosen to represent a decrease of PSI, and numbers
753 of exon junction reads were indicated. (E) The hit top enriched motifs identified in the
754 differentially spliced genes regulated via RBM7. (F) RBM7-regulated exon skipping
755 events were identified by semiquantitative RT-PCR using RBM7-konckdown or control
756 MDA-MB-231 cells. The mean ± SEM from 3 experiments was plotted. P values of
757 percent-spliced-in (PSI) values were determined by one-way ANOVA with Dunnett's
758 multiple comparisons test. (G) Gene Ontology analysis showed that the significant
759 splicing events affected biological process upon RNM7 knockdown in MDA-MB-231
760 cells. (H) KEGG pathway enrichment of the RBM7-mediated AS targets.
761

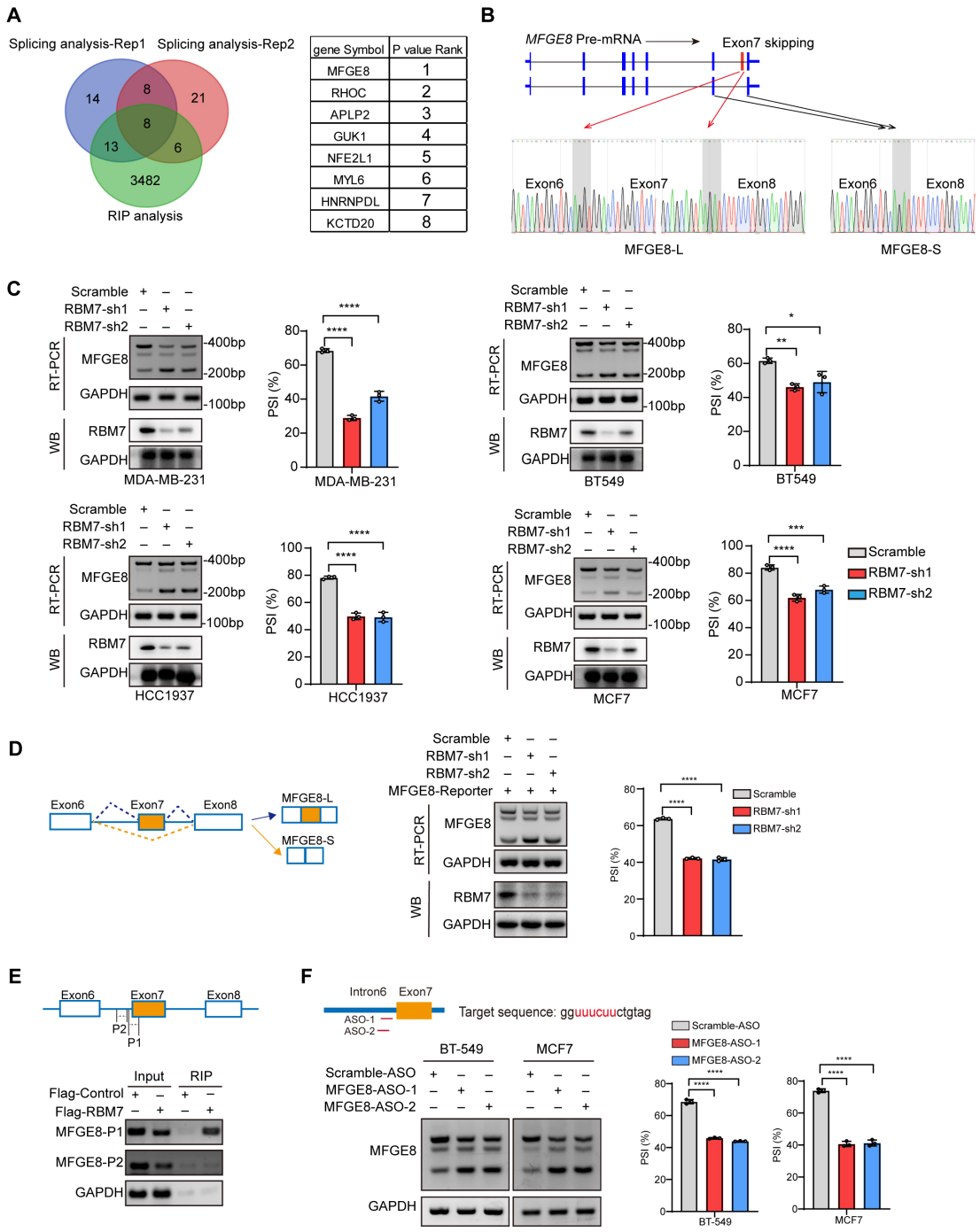

Figure 4. RBM7 knockdown promoted MFGE8 exon 7 skipping via binding to its pre-mRNA. (A) Venn diagram of 3509 RBM7-binding genes from the RIP-seq (based on data set GSE144075), 43 genes in RBM7-sh1 cells compared with control cells, and 43 genes in RBM7-sh2 cells compared with control cells. The gene lists of the last two groups were from RNA sequencing with top 50 AS events. The gene lists on the right

768 were shown according to the P value. (B) Schematics of human MFGE8 pre-mRNA
769 (NM_005928.4). And MFGE8-long isoform included the exon 7 (hereafter referred to
770 as MFGE8-L), while MFGE8-short isoform skipped the exon (hereafter referred to as
771 MFGE8-S). The arrow indicates the direction of transcription. Primers were designed
772 on the upstream and downstream exons of exon 7, and RT-PCR was performed to
773 identify MFGE8 splicing event using RBM7-KD cells or control MDA-MB-231 cells.
774 The PCR products were subjected to sanger sequencing. The base peak diagram of
775 sanger sequencing showed the splicing junction sites (filled with gray) of upstream and
776 downstream exon 7. (C) Different breast cancer cells lines with stable low-expression
777 of RBM7 or control were constructed. Alternative splicing events of MFGE8 regulated
778 by RBM7 were examined by semi-quantitative RT-PCR. The level of RBM7 protein
779 was detected by Western Blotting assay in various cell lines. The mean ± SD of PSIs
780 from three independent repeated experiments were plotted. P value was calculated by
781 one-way ANOVA with Dunnett's multiple comparisons test. (D) As schematic diagram,
782 an exon of the orange box is a variable exon as shown in the diagram. P1 and P2 were
783 the putative binding regions and primers were designed here. Binding of MFGE8 pre-
784 mRNA with RBM7 was examined by RNA- immunoprecipitation (RIP) in HEK293T
785 cells expressing Flag-RBM7 or Flag-empty plasmid. (E) The diagram shows ASOs
786 targeting the indicated region. MCF7 and MDA-MB-231 cells were transfected with
787 MFGE8-ASO for 48h. And then MFGE8 splicing events were measured by RT-PCR.
788 (F) Schematics of human MFGE8 mini splicing reporter gene and the reporter
789 contained 3 exons and two mini-introns. RBM7 stable knockdown cells or control cells

790 were transfected with mini reporter gene, and RNA was collected 24 hours of
791 transfection. The splicing changes of exogenous MFGE8 were detected by RT-PCR
792 with specific primers on the reporter gene. The level of RBM7 protein was detected in
793 MCF7 cells by Western blotting assay. P value was calculated by one-way ANOVA
794 with Dunnett's multiple comparisons test from three repeated experiments.

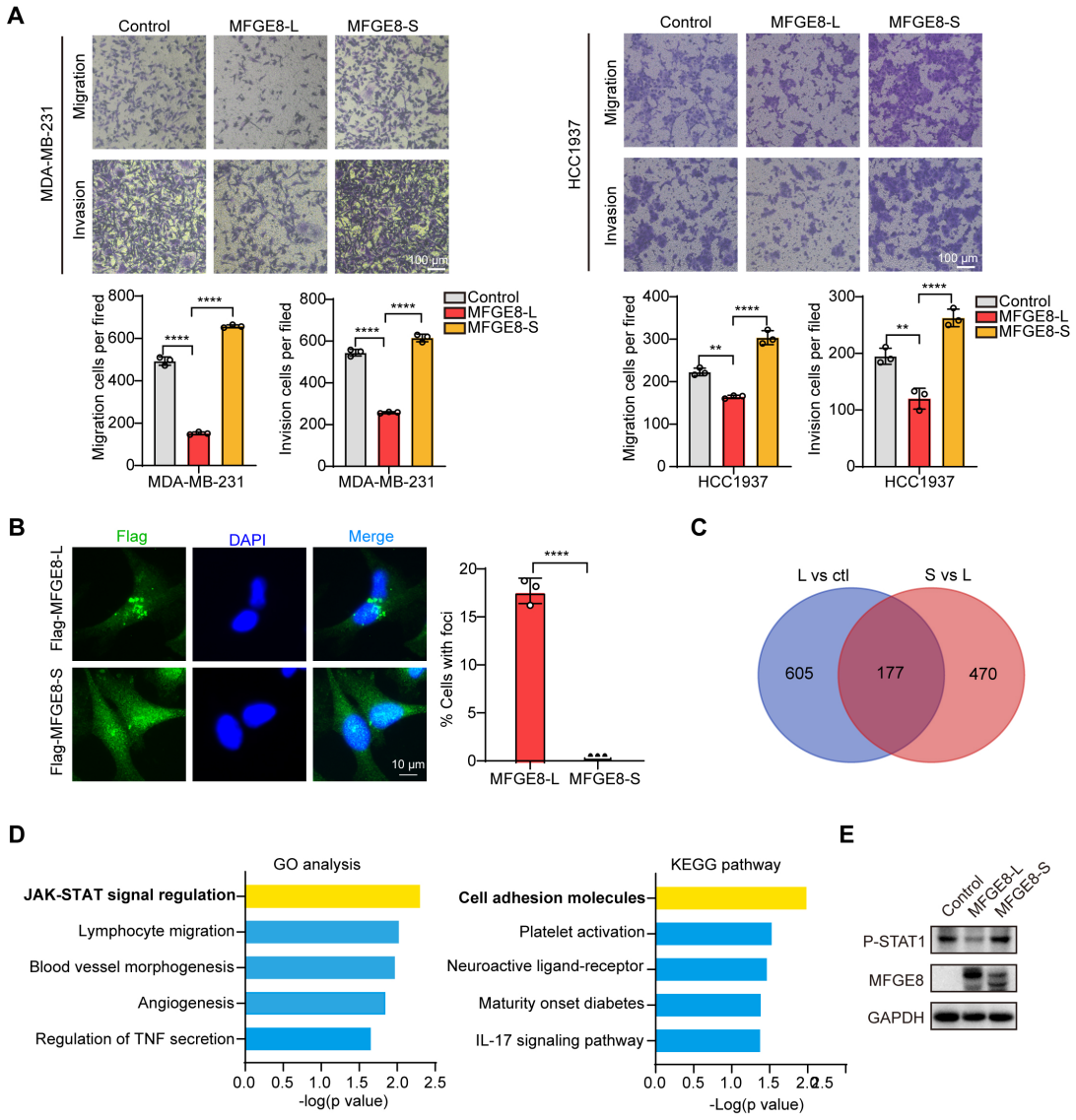

Figure 5. MFGE8-L inhibited breast cancer cell motility and invasion. (A) Effects of MFGE8 two isoforms on breast cancer cell migration and invasion were evaluated by Transwell assays. (B) The subcellular localizations of MFGE8 isoforms. MDA-MB-231 cells were transfected with Flag-tagged MFGE8-L or MFGE8-S, and visualized with immunofluorescence assay. Scale bar = 10 μm. The localization of MFGE8-L and MFGE8-S was quantified with foci, and the percent of cells were plotted (about 80 cells were captured and quantified in both samples). (C) Transcriptome sequencing was performed using MDA-MB-231 cells of overexpressing MFGE8-L and MFGE8-S.

804 Venn diagram of 782 MFGE8-L down-regulated genes, 647 genes from MFGE8-S up-
805 regulated genes compared with MFGE8-L. (D) Gene ontology analysis and KEGG
806 pathway analysis of genes up-regulated by MFGE-S compared with MFGE8-L. (E) The
807 expression of MFGE8 and p-STAT1(Tyr701) in HCC1937 cells overexpressing
808 respectively MFGE8-L and MFGE8-S was detected by Western Blotting assay.
809

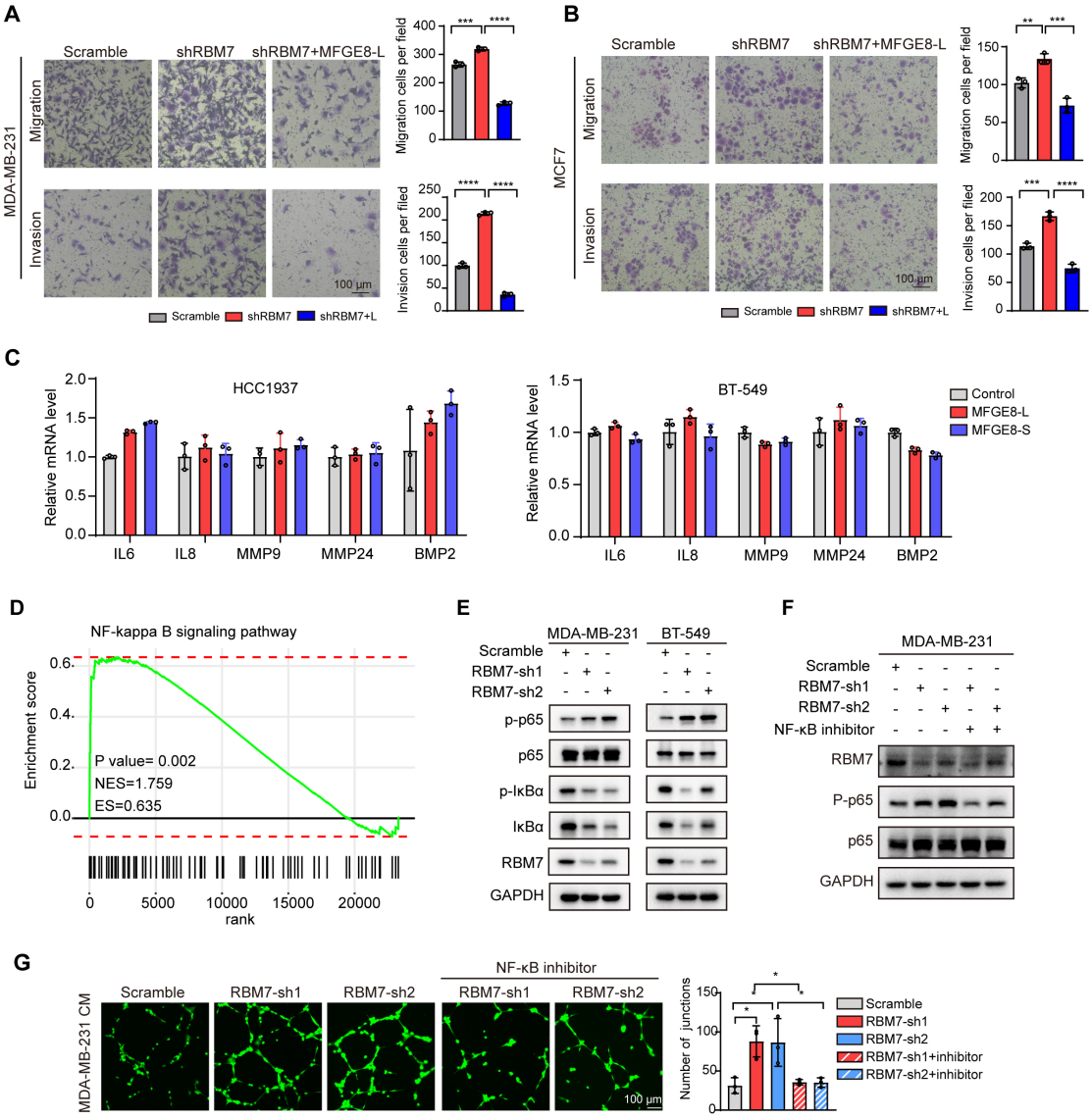

Figure 6. RBM7 knockdown enhanced aggressiveness of breast cancer relying on MFGE8 splicing switch to the short variant and NF-κB pathway activation. (A-B) Breast cancer cells MDA-MB-231 (A) and MCF7 (B) were transfected with shRBM7 or control and re-transfection Flag-MFGE8-L vector. Then these cells were subjected to Transwell migration assay or invasion assay. Cells migrating through Transwell membrane with matrigel or not were imaged and representative images are shown (right) along with quantification (left). (C) HCC1937 and BT-549 cells stably expressing MFGE8-L, MFGE8-S and control were generated. The expression of metastasis-related

819 inflammatory factors was measured by real-time PCR assay. (D) NF-κB signaling
820 pathway was enrichment via KEGG analysis in RBM7 knockdown cells. (E) Western
821 blotting showed the expression of NF-κB-associated proteins in RBM7-depleted or
822 control MDA-MB-231 and BT-549 breast cancer cell lines. (F) RBM7-depleted MDA-
823 MB-231 cells were treated with or without NF-κB inhibitor PDTC 10 μm for 48h. Then
824 Western blotting tested the expression of RBM7, NF-κB -p65 and phosphorylated NF-
825 κB p65. (G) Representative images of the tube formation of HUVEC cells, treated with
826 conditional medium with 10 μm NF-κB inhibitor PDTC. Scale bars: 100 μm.
827 Quantification of junctions was by imageJ software.
828

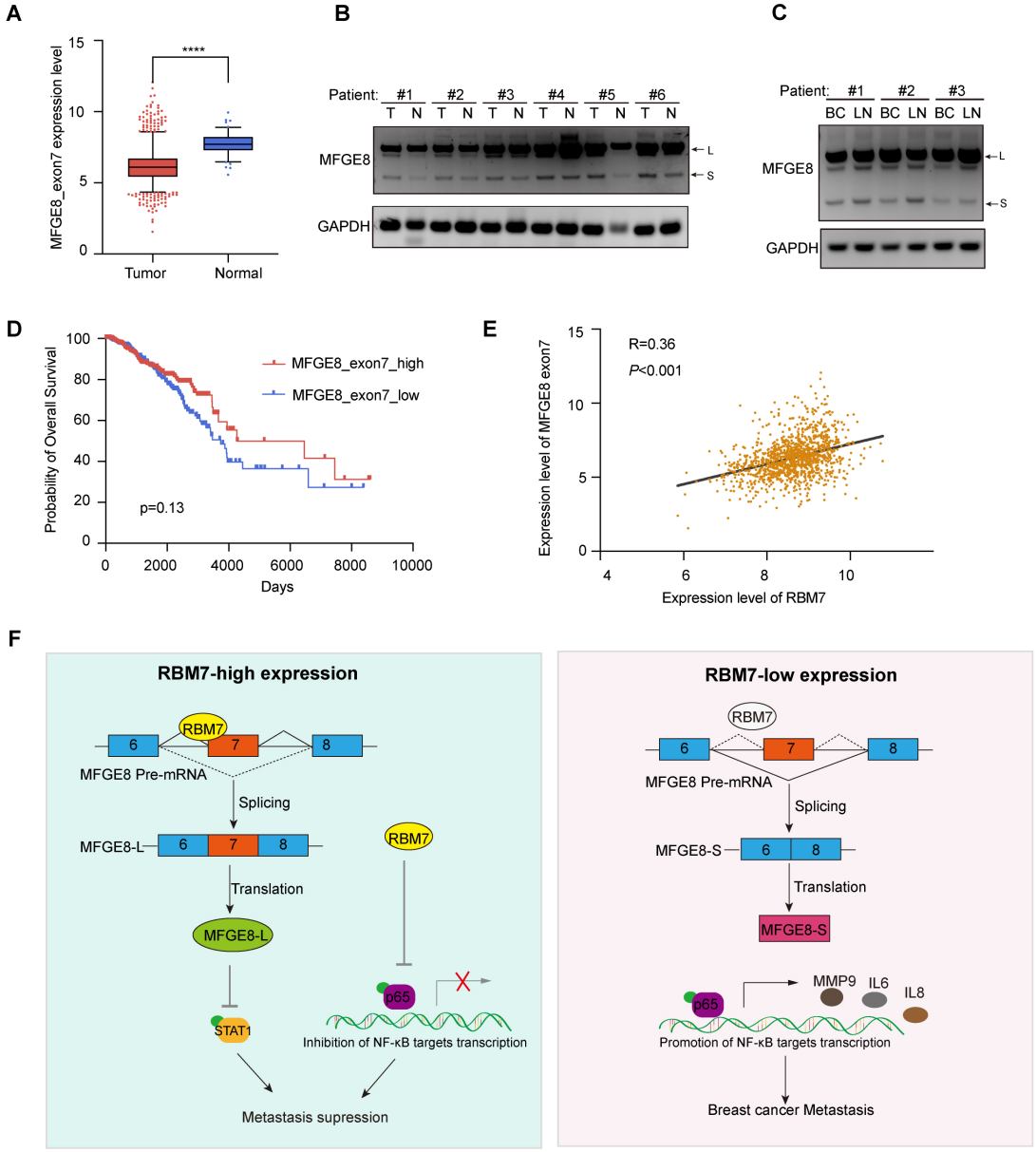

Figure 7. Splicing shift of MFGE8 toward exon7 exclusion was negatively correlated with RBM7 expression in patients with breast cancer.

(A) MFGE8_exon7 expression level was analyzed in breast carcinoma from the TCGA dataset. (B-C) MFGE8 alternative splicing events were quantified in 6 pairs of primary BRCA tissues and adjacent normal tissues using RT-PCR (B). Semi-quantitative RT-PCR was performed using 3 pairs of primary breast cancer tissues and lymph node metastasis of breast cancer tissues (C). (D) Correlation of RBM7 with the MFGE8

837 exon7 expression levels was analyzed with Pearson's correlation coefficient. (E) The
838 correlation between MFGE8-S and overall survival (OS) of breast cancer patients based
839 on the TCGA dataset. (F) The mechanistic model of this study. Schematic illustration
840 of the roles of RBM7-MFGE8 splicing switch axis in metastasis of breast cancer.
841

Supplementary Figure 1

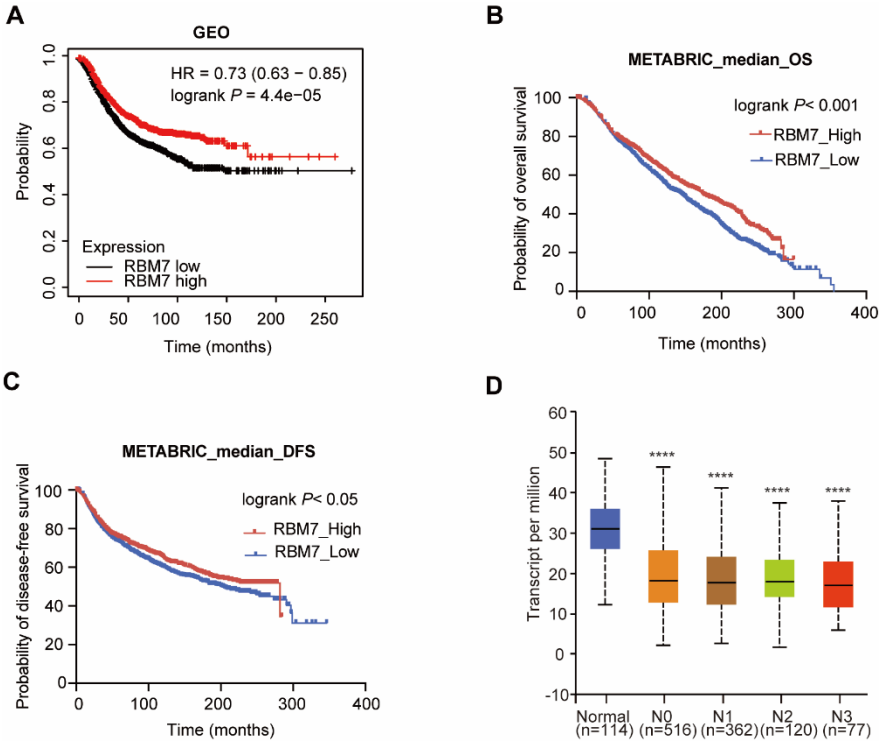

Supplement Figure1.The low expression of RBM7 in breast cancer was positively correlated with the poor survival of patients.

(A)The correlation between RBM7 expression and overall survival of breast cancer patients based on data from the Kaplan–Meier Plotter cohort. (B-C) METABRIC analysis of the correlation between RBM7 expression and overall survival (OS) and disease-free survival (DFS) of breast cancer patients based on the METABRIC dataset. The p value was obtained by log-rank test (A, B, C). (D) RBM7 mRNA level was analyzed in breast invasive carcinoma based on nodal metastasis status from the UALCAN dataset. The p-value was calculated by unpaired Student's t-test by comparing lymph node metastasis of breast cancer tissues with normal tissue.

Supplementary Figure 2

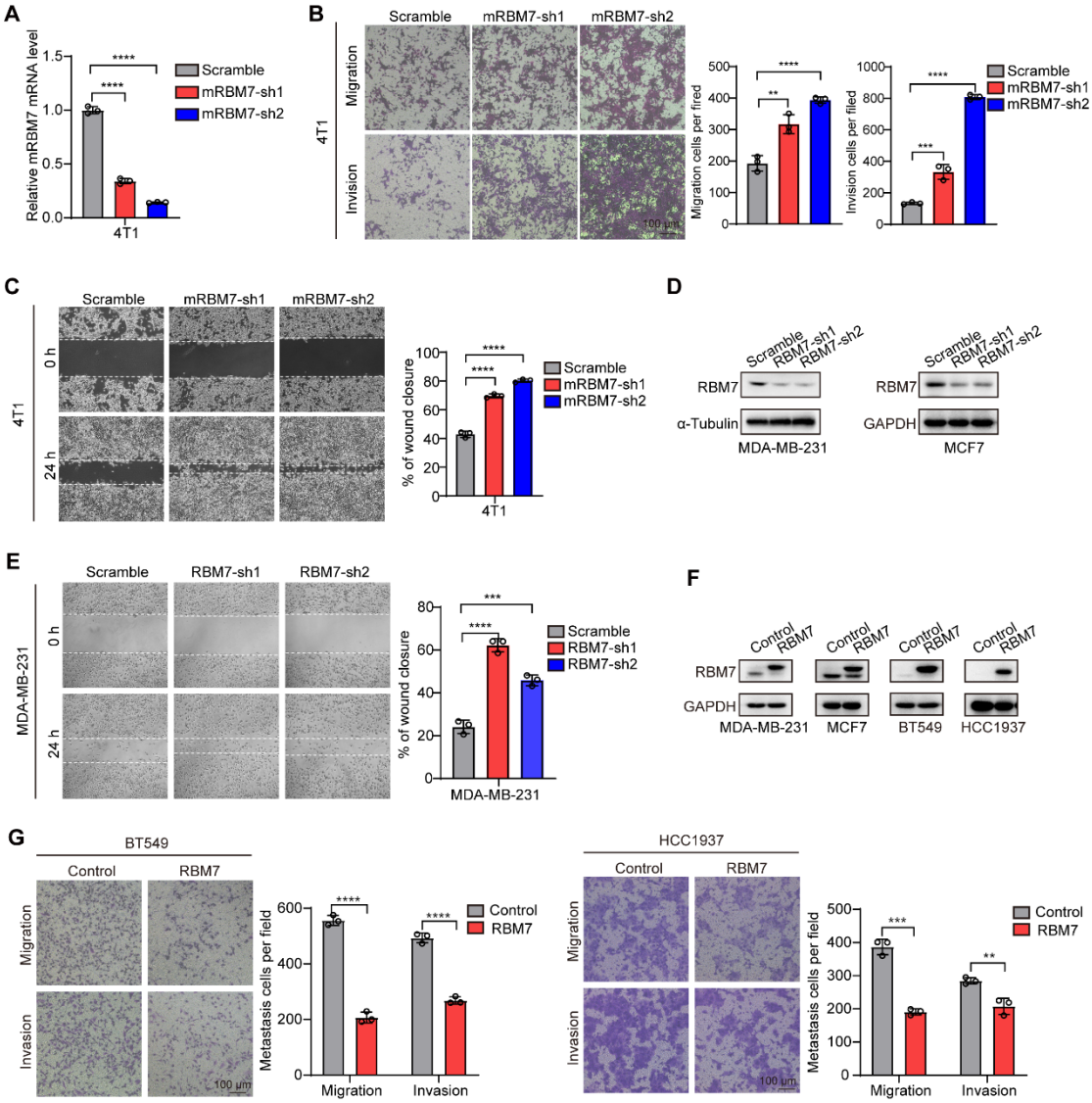

Supplement Figure2. RBM7 inhibited breast cancer cell migration and invasion. (A) The mouse cell line with RBM7 knockdown was constructed. And the expression of RBM7 was detected by real-time quantitative PCR. (B) The migration and invasion ability of murine RBM7 was detected by Transwell assay using RBM7-KD 4T1 cells. (C) The metastatic capability of RBM7 on 4T1 cells was evaluated by wound healing assay. (D) Western blotting showed the expression of RBM7 in MDA-MB-231 cells and MCF7 cells of RBM7-depleted. (E) The metastatic capability of RBM7 on MDA-MB-231 cells was evaluated by wound healing assay. (F) Western blotting showed the expression of RBM7 in various breast cancer cell lines of RBM7 over-expression. (G) The metastatic ability of RBM7 for BT-549 cells and HCC1937 cells of promoted expression of RBM7 was evaluated by Transwell assay. Data are mean ± SD from three random fields. P values were determined by unpaired Student's T test (G). P value was calculated by one-way ANOVA with Dunnett's multiple comparisons test (A, B, C, E).

Supplementary Figure 3

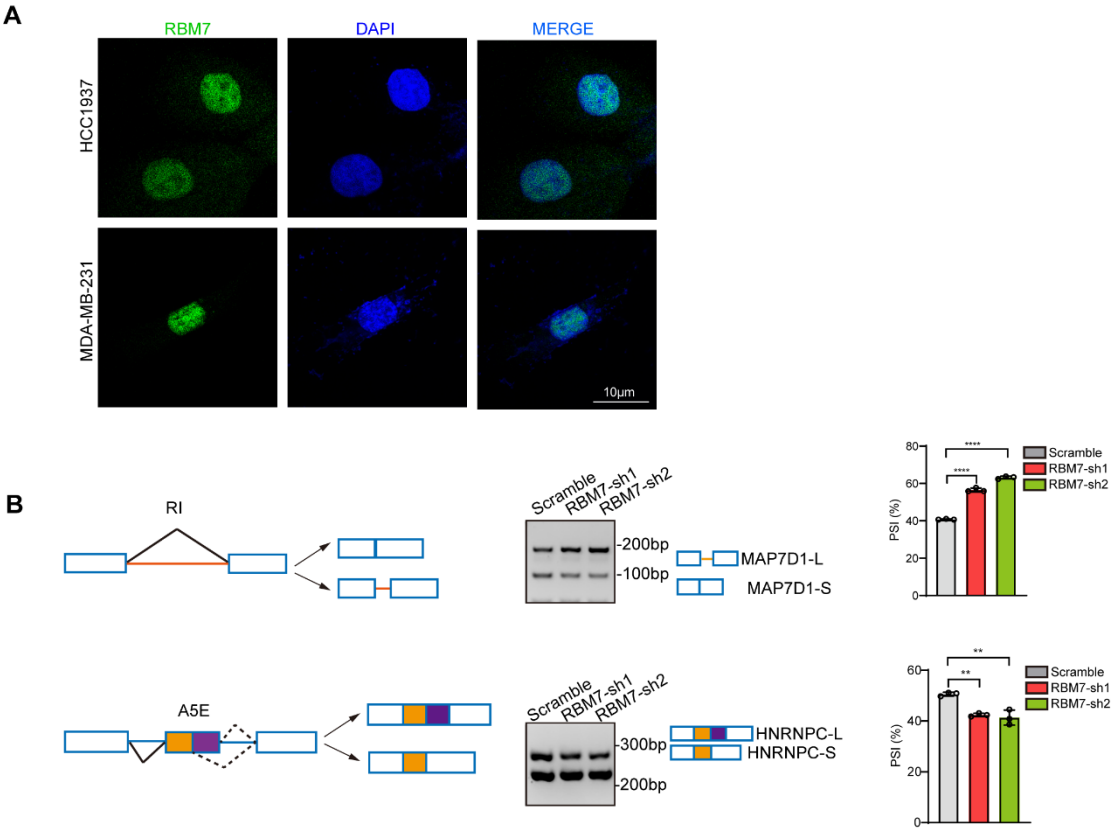

Supplement Figure3. RBM7 could regulate alternative splicing in breast cancer cells.

(A) Representative image of MDA-MB-231 and HCC1937 cells stained for RBM7. Scale bar=10 μm. (B) Semi-quantitative RT-PCR was performed to validate the AS events in MAP7D1, and HNRNPC in MDA-MB-231 cells with RBM7 knockdown compared with controls. P value was calculated by one-way ANOVA with Dunnett's multiple comparisons test.

Supplement Figure 4

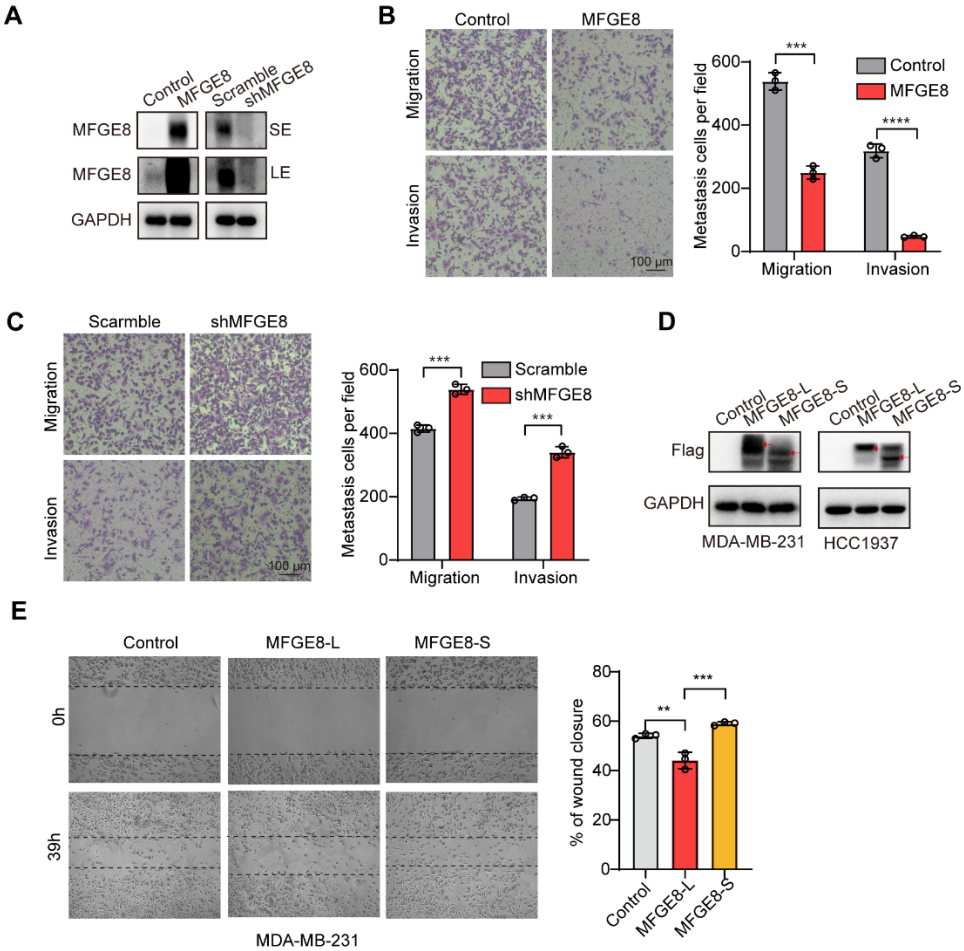

Supplement Figure4. MFGE8-L suppressed breast cancer cells migration and invasion.

(A) The protein expression of endogenous MFGE8 was determined by western blot in MDA-MB-231 cells knocking down or over-expression MFGE8. SE denotes long exposure and LE denotes long exposure. (B-C) Transwell assay with Matrigel or not was performed using MFGE8 promoted MDA-MB-231 cells or MFGE8 decreased expression cells. P value was calculated by unpaired Student's T test. (D) Western blot showed the extrinsic expression of MFGE8-L isoform and MFGE8-S isoform in MDA-MB-231 and HCC1937 transfected respectively Flag-MFGE8-L, Flag-MFGE8-S and empty vectors. The red arrow indicates the location of the protein. (E) MDA-MB-231 cell line expressing MFGE8-L, MFGE8-S or a vector control were analyzed by wound healing assay. Percent of wound closure was measured in triplicate experiments, with mean ± SD plotted (p values were calculated by one-way ANOVA with Tukey's multiple comparisons test).

Supplement Figure 5

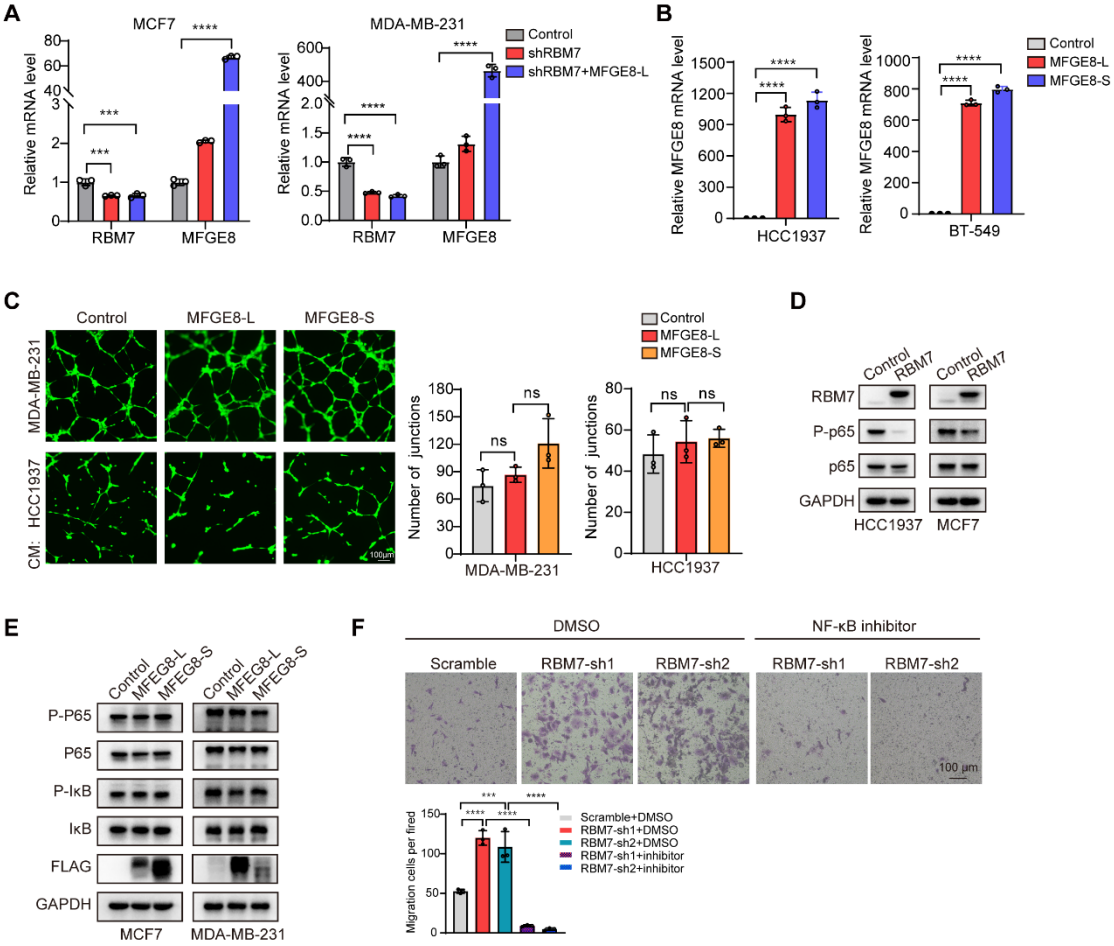

Supplement Figure5. MFGE8-L/S isoforms had no effect on NF-κB pathway in breast cancer cells.

(A) MCF7 and MDA-MB-231 cells stably expressing shRBM7, shRBM7/MFGE8 and control were generated. The expression of RBM7 and MFGE8 was measured by real-time PCR assay. The mean ± SD of relative mRNA levels from triplicate experiments are plotted. (B) HCC1937 and BT-549 cells stably expressing MFGE8-L, MFGE8-S and control were generated. The expression of MFGE8 was measured by real-time PCR assay. (C) Representative images of the tube formation of HUVEC cells, treated with conditional medium, which cultured MFGE8-L, MFGE8-S stably transfected cells and control cells for 48h and collected. Scale bars: 100 μm. Quantification of junctions was by imageJ software. (D) Western blotting showed the expression of indicated proteins in RBM7-promoted or control breast cancer cells. (E) Western blotting showed the indicated antibodies in up-expression of MFGE8 different isoforms in breast cancer cells. (F) RBM7-depleted MDA-MB-231 cells were treated with or without NF-κB inhibitor PDTC 10 μm for 48h. Then Transwell assays were performed to assess cell migration ability. p values were calculated by one-way ANOVA with Tukey's multiple comparisons test (C, F).

Supplement Figure 6

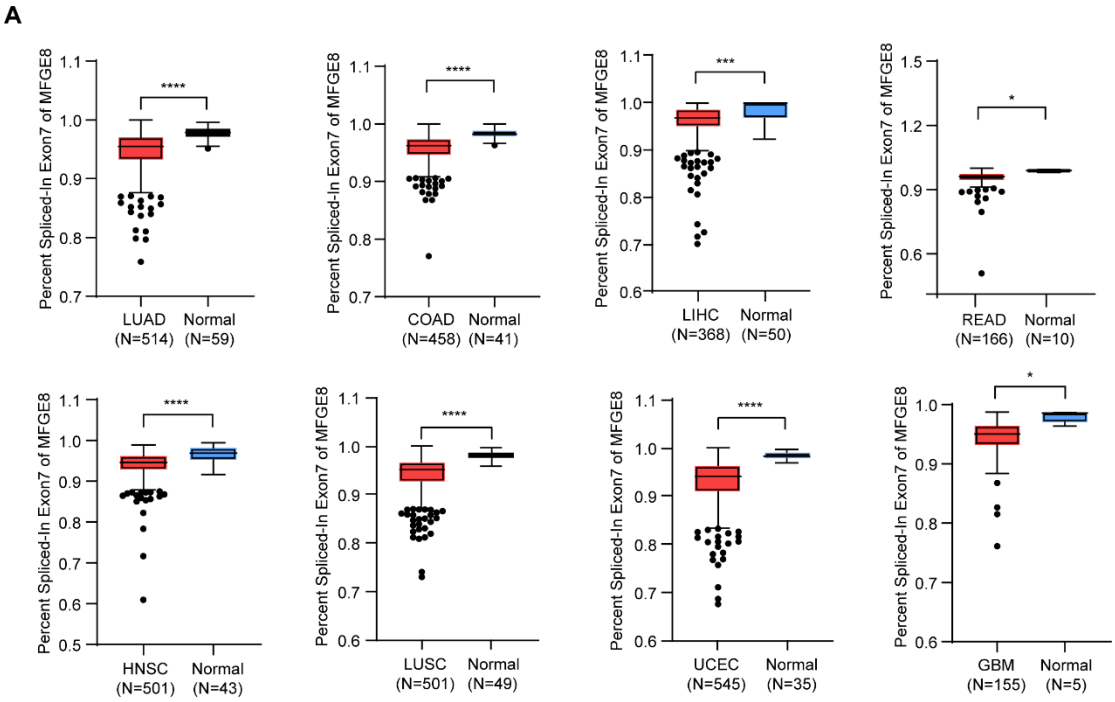

Supplement Figure6. MFGE8 exon7 skipping is enhanced in a variety of cancers. (A) MFGE8_exon7 skipping event was analyzed in various cancers according to TCGA SpliceSeq dataset. The p-value was calculated by unpaired Student's t-test.

Primers	Gene	primer name	sequence
Primers for qRT-PCR	RBM7	RBM7-qF	5'-AAGCGGATCGCACTCTCTTT-3'
		RBM7-qR	5'-ACGCAAACTGCTTTGGTTTAC-3'
	GAPDH	GAPDH-qF	5'-ATGGGGAAGGTGAAGGTCG-3'
		GAPDH-qR	5'-GGGGTCATTGATGGCAACAATA-3'
	MFGE8	MFGE8-qF	5′-TTCCCAAGAAGTGCGAGGAGATGT-3'
		MFGE8-qR	5′-ATGCTGCAAACCCAAGAAGGTCAC-3'
	IL6	IL6-qF	5′-GAAAGCAGCAAAGAGGCAC-3'
		IL6-qR	5′-GCTCTGGCTTGTTCCTCACTAC-3'
	BMP2	BMP2-qF	5'-TCGCAGGCACTCAGGTCAG-3'
		BMP2-qR	5'-TTCCCACTCGTTTCTGGTAGTT-3'
	MMP9	MMP9-qF	5'-AACTTTGACAGCGACAAGAAGT-3'
		MMP9-qR	5'-ATTCACGTCGTCCTTATGCAAG-3'
	IL8	IL8-qF	5'-GTGCAGTTTTGCCAAGGAGT-3'
		IL8-qR	5'-CTCTGCACCCAGTTTTCCTT-3'
	MMP24	MMP24-qF	5'-ATCTGCTTCCCTATGACTCACG-3'
		MMP24-qR	5'-CGCTTGTTTCTCCGCCTAC-3'
	mGAPDH	mGAPDH-qF	5'-CCTTCCGTGTTCCTACCCC-3'
		mGAPDH-qR	5'-GCCCTCAGATGCCTGCTTC-3'
	mRBM7	mRBM7-qF	5'-GTGTCTGTTCCCTATGCC-3'
		mRBM7-qR	5'-CACGTTACCCACTGTCCT-3'
Primers for alternative splicing	MFGE8	MFGE8-SE-F	5'-TGGGCCTGAA GAATAACA-3'
		MFGE8-SE-R	5'-CAAGTTCTTCTTGTGGGA-3'
	AKT2	AKT2-SE-F	5'-GCGTGTCTTCACAGAGGAGC-3'
		AKT2-SE-F	5'-AGCCCAGCAAGCAGGGACT-3'
	ZMYND8	ZMYND8-SE-F	5'-ACCCTTGACCTTTCTGGCT-3'
		ZMYND8-SE-R	5'-CCAGCCGAGACTCTTTCG-3'
	MBNL1	MBNL1-SE-F	5'-TACCAACGTG GCAATTGC-3'
		MBNL1-SE-R	5'-TAATGGGGGAAGTACAGCTT-3'
	MAP7D1	MAP7D1-RI-F	5'-ATCGCAGCCTGCAGCTGA-3'
		MAP7D1-RI-R	5'-TGCACGCTTCGGGTGACGCT-3'
	HNRNPC	HNRNPC-A5E-F	5'-GGCTTTGCCTTCGTTCAG-3'
		HNRNPC-A5E-R	5'-CATCCTATCATAATAGTCCCGTTG-3'